



Phase Equilibria in the Zr-Ti-Cu System

Anastasiia Storchak¹ · Vasyly Petuykh¹ · Victor Sobolev² · Iryna Tikhonova¹ · Marina Bulanova¹

Submitted: 5 April 2023 / in revised form: 7 June 2023 / Accepted: 7 June 2023 / Published online: 27 November 2023
© ASM International 2023

Abstract Phase equilibria in the Zr-Ti-Cu system have been studied by differential thermal analysis, scanning electron microscopy, x-ray microanalysis, and x-ray diffraction. Based on the obtained results, a ternary phase diagram was constructed over the entire composition range in the crystallization interval. The results are presented in the form of liquidus and solidus projections, the Scheil reaction scheme, and isopleths for sections of 40 and 70 at. % Cu. Phase equilibria in the system are defined by the ternary compound $ZrTiCu_2$ (τ_1) and the binary-based phase $Zr_{14}Cu_{51}$. These phases have the widest fields of primary crystallization on the liquidus projection and form two-phase equilibria with all other phases on the solidus projection. The solidus projection contains 11 three-phase fields. Two of them form by invariant four-phase reactions of the transition type, the rest by eutectic ones. A comparison of the solidus projection with the published isothermal sections at 800 and 750 °C led to the need for two solid-state four-phase invariant equilibria involving binary Ti-Cu intermetallic compounds. They are shown to occur between 840 and 850 °C. The ternary compound $Zr_{22}Ti_{14.5}Cu_{63.5}$ (τ_2) was shown to form in the solid state at 827 °C by three-phase invariant reaction $\tau_1 + Zr_{14}Cu_{51} \rightleftharpoons \tau_2$.

Keywords crystallization · liquidus projection · solidus projection · Zr-Ti-Cu

1 Introduction

The first interest in the Zr-Ti-Cu system is associated with the search for eutectoid-forming alloys with good mechanical characteristics.^[1] This concerns the composition region Zr-Zr₂Cu-Ti₂Cu-Ti, where eutectoid transformation ($\beta Zr, \beta Ti$) \rightleftharpoons ($\alpha Zr, \alpha Ti$) + (Zr,Ti)₂Cu (γ -phase) occurs. However, the main ongoing interest in this system since the 1980 s is caused by finding the bulk glass forming ability in multicomponent Zr-, Ti- and Cu-based alloys^[2-5] and others, which possess a combination of attractive properties. Based on the boundary binary systems, the possibility of glass formation by rapid quenching in ternary Zr-Ti-Cu alloys in a wide composition range was suggested by (Ref 6) which was later confirmed by many authors^[7-14] and others.

This resulted in numerous studies of phase equilibria in Zr-Ti-Cu system. Most of them concerned partial and complete experimentally determined isothermal sections at 700 to 800 °C.^[1,6,15-22] CALPHAD assessments of the system were performed by (Ref 23, 24). Few works^[21,25-27] considered ternary compounds.

Experimental data on phase equilibria with participation of the melt is scarce. Thus, as-cast samples were studied in (Ref 28) the liquidus and solidus projections in the subsystem Zr-Zr₂Cu-Ti₂Cu-Ti were plotted by (Ref 29). Meanwhile, as amorphous alloys are obtained by the melt spinning technique, knowledge of the processes taking place in the crystallization interval becomes important.

Thus, in this work we report our results from experimental study of the solidus and liquidus projections of the system. Solid-state transformations, which occur between the solidus temperatures and 750 °C^[21] are discussed, as well. Since the subsystem Zr-Zr₂Cu-Ti₂Cu-Ti was

✉ Anastasiia Storchak
asyasf@bigmir.net

¹ Frantsevich Institute for Problems of Materials Science NAS of Ukraine, Kyiv, Ukraine

² Technical Center NAS of Ukraine, Kyiv, Ukraine

considered by us in (Ref 29) we focus here on the subsystem Zr_2Cu - Cu - Ti_2Cu .

The data on phase equilibria in the system and on related questions published before 2004 were assessed in (Ref 30). However, most of the papers on the subject were published after 2004. So, brief evaluation of the data concerning phase relations in the system seems desirable.

2 Literature Evaluation

The boundary binary phase diagrams are shown in Fig. 1 according to^[31] (Ti-Cu) and^[32] (Zr-Ti, Zr-Cu).

The first study of the system was performed by Ence and Margolin,^[1,15] where partial isothermal section at 750 °C for Ti-corner was experimentally determined and predicted for Zr-corner. The existence of a continuous solid solution between Zr_2Cu and Ti_2Cu (here γ -phase) was suggested. Later this was experimentally established at 700 °C by (Ref 16) and repeatedly confirmed.^[17-20, 22, 29, 33]

Chebortnikov and Molokanov^[33] experimentally determined the vertical section Zr_2Cu - Ti_2Cu and claimed that it is not quasibinary. The same conclusion results from experimental data^[6] and thermodynamic calculation,^[23] which is based on data from (Ref 6). Whilst, according to thermodynamic calculation^[24] and our data,^[29] the section is quasibinary. The reason for this discrepancy is based on different versions of Ti-Cu phase diagram used by different authors, where Ti_2Cu compound was shown to melt either congruently or incongruently. In (Ref 29) we have experimentally shown the congruent melting of Ti_2Cu . The section Zr_2Cu - Ti_2Cu , thus, is quasibinary, and the system Zr-Ti-Cu can be divided into two subsystems. It was assumed that the section of^[33] might not pass strictly through the composition of Ti_2Cu , and, thus, was not quasibinary.

According to experimental results^[18,29] and thermodynamic calculation,^[24] the γ -phase has insignificant homogeneity range with respect to copper (below 2 at.%). In the subsystem Zr- Zr_2Cu - Ti_2Cu -Ti the solidus surface is characterized by coexistence of γ and (βZr , βTi) (β -phase) in the entire composition region. Subsequently, the liquidus surface is formed by the fields of primary crystallization of these phases, separated by the monovariant eutectic curve $L \rightleftharpoons \beta + \gamma$. The solidus temperature has a minimum and in this point the above three-phase equilibrium becomes invariant.

The β and γ phases coexist in wide composition ranges below the solidus, as well, as shown in the isothermal sections at 703,^[22] 750^[19,20] and 800 °C.^[17,18] The same result was obtained in CALPHAD modeling.^[23,24]

In contrast,^[6] shows an alternative two-phase equilibrium β +ternary Laves phase (here τ_1) at 703 °C. In turn, Zr_2Cu and Ti_2Cu should not form a continuous solid solution. This result was later shown to be incorrect.

The ternary Laves phase $ZrTiCu_4$ with $MgZn_2$ structure type was found by (Ref 25, 26). Later, its composition was corrected as $ZrTiCu_2$ by (Ref 6) and confirmed in subsequent works.^[27] Refined the crystal structure of the compound. According to^[2,6] and thermodynamic assessments,^[23,24] the phase melts congruently. The melting temperature at stoichiometric composition was experimentally established as 867 °C,^[2] who plotted the isopleth ZrCu-TiCu. The temperature 883 °C was calculated by (Ref 23). According to^[6] and subsequent works, τ_1 phase has wide homogeneity range. The limits of the homogeneity range of the phase, as measured by different authors at different temperatures, are compared in Table 1. As one can see, these data agree well with each other. Some question arises concerning high Zr solubility in τ_1 phase at 827 °C.^[2]

Available isothermal sections, both experimental and calculated, agree well on the main features. Thus, in the

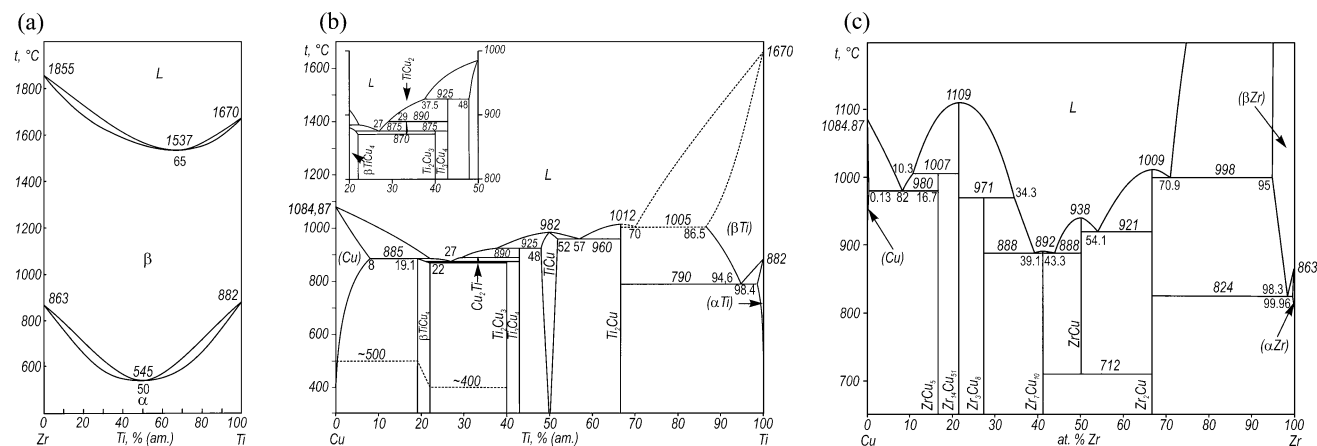


Fig. 1 Phase diagrams of the boundary binary systems: (a) Ti-Zr^[32] (b) Ti-Cu^[31] (c) Zr-Cu^[32]

subsystem Zr_2Cu -Cu- Ti_2Cu the phases τ_1 and $Zr_{14}Cu_{51}$ participate in two-phase equilibria with all other phases and, thus, define the character of phase equilibria. Subsequently, three-phase fields, established by different authors, are mostly similar. Some discrepancies are, however, present concerning the character of three-phase regions with participation of Zr-Cu compounds. For instance, τ_1+ZrCu equilibrium is reported for 703^[6, 24] and 800 °C,^[17, 18, 22, 24] however, it was not found at 750 °C.^[19, 21] These discrepancies result from different solubilities of Ti in the above compounds established by different authors. Other inconsistencies in the results of different authors, even for the same temperatures, concern the location of the corners of some three-phase fields.

Note that the isothermal section at 703 °C of^[6] significantly differs from the others. Most of these differences were eliminated in subsequent works, where the section at this temperature was experimentally determined^[22] and calculated.^[23, 24]

However, a major difference exists between the isothermal section at 750 °C^[21] and the other works. In this work one more ternary compound τ_2 was found. The composition of the compound was established as $Zr_{22}Ti_{14.5}Cu_{63.5}$. The width of the homogeneity range of the phase does not exceed 1 at.%. The crystal structure was not resolved; however, it was established that it is hexagonal with cell size 12×9.8 Å. The formation mechanism of this phase was not established.

In (Ref 2) the isopleths ZrCu-TiCu was constructed. The section τ_1 -TiCu is shown as quasibinary of eutectic type, while in the ZrCu- τ_1 part crystallization of ternary eutectic $\tau_1+\gamma+Zr_{14}Cu_{51}$ is shown. However, this part represents a violation of the Gibbs' phase rules. Note: that $Zr_{14}Cu_{51}$ compound is named $ZrCu_{3.6}$.

3 Experimental

The starting materials for the preparation of alloys were electrolytic copper (99.99% (wt.)), iodide titanium (99.94% (wt.)) and zirconium (99.96% (wt.)). The alloys were melted in a vacuum arc furnace with a non-consumable tungsten electrode on a water-cooled copper hearth in an argon environment (pressure ~ 80 kPa). The atmosphere was additionally purified by molten titanium getter for at least 5 min. The ingots were turned over and remelted twice to homogenize the chemical composition of the samples. The mass of the ingots was about 10 g. The cooling rate of the ingots on the bottom of the furnace was ~ 100 °C/s. Mass losses during melting did not exceed 0.2% (wt.). Measurements of the composition of selected samples by local x-ray spectral analysis confirmed their agreement with the initial mixtures. The content of impurities (O, N, Ni, Zr, Si) according to chemical and spectral analyzes, measured on selected alloys, did not exceed 0.01% (wt.).

Temperatures of phase transformations were determined by differential thermal analysis (DTA) in the device with a tungsten-rhenium thermocouple W/WRe20.^[34] Al, Ag, Au, Pd, Fe references were used to calibrate the thermocouple. The calibration error was ± 5 °C. Heating/cooling rates of ~ 20 or 40 °C/min were used. The experiments were carried out in He grade A atmosphere. Samples weighing up to 1.0 g were placed in Al_2O_3 or Sc_2O_3 crucibles. The investigation was conducted on cast and previously annealed (750 °C/536 h^[20]) samples. The reproducibility of the data regarding the temperature of thermal effects was ± 3 °C.

For microstructural investigation the samples were polished using an aqueous suspension of Cr_2O_3 . The microstructure of alloys and the composition of phases were determined by scanning electron microscopy (SEM)

Table 1 Limits of the homogeneity range of the ternary Laves phase

Direction Zr-Ti system-Cu, at.% Cu		Direction Zr-Cu system-Ti-Cu system, at.% Zr		Temperature, °C	Comments	Reference
Minimal	Maximal	Minimal	Maximal			
...	...	22.5	29	627	Isoconcentrate 50Cu	2
45	50	25	30	703		6
		23	31	703		22
46	52	21	29	750		19
42.5	50.5	23	33	750		20
44	52	21	30	800		18
44	52	20	31	800		17
44	52	800	Ray 50Zr50Ti-Cu	27
...	...	21	37 ¹	827	Isoconcentrate 50Cu	2

¹Questionable value.

and local x-ray spectral analysis (LRSA) on Superprobe–733 and Superprobe–8200 devices. Pure copper, titanium and zirconium were used as standards.

Diffraction patterns were obtained on a DRON-3 device from metallographic sections using filtered Cu K α radiation. The range of 2 θ angles was 20–100°, the scanning step was 0.05–0.1°, and the exposure was 2 sec. The results were analyzed using the PowderCell software package. The lattice parameters were calculated by an iterative least squares method.

Several samples previously annealed at 750 °C/536 h^[20] were additionally annealed near solidus temperatures in an SShVL-0.6.2/16 resistance furnace. Each sample was placed in an Al₂O₃ crucible. These samples were studied by microscopy and microprobe methods.

4 Results and Discussion

4.1 Liquidus Projection

The liquidus projection of the Zr–Ti–Cu system is shown in Fig. 2. The part with less than 33.3 at.% Cu is adopted from (Ref 29). The liquidus temperatures along the section Zr₂Cu–Ti₂Cu are taken from (Ref 24). The part with more than 33.3 at.% Cu results from this investigation.

In the subsystem Zr₂Cu–Cu–Ti₂Cu, the liquidus projection is characterized by the presence of primary crystallization fields of γ , (Cu), τ_1 and all phases based on Zr–Cu and Ti–Cu compounds which form with the participation of the melt in the binary systems. On the contrary,^[23, 24] show

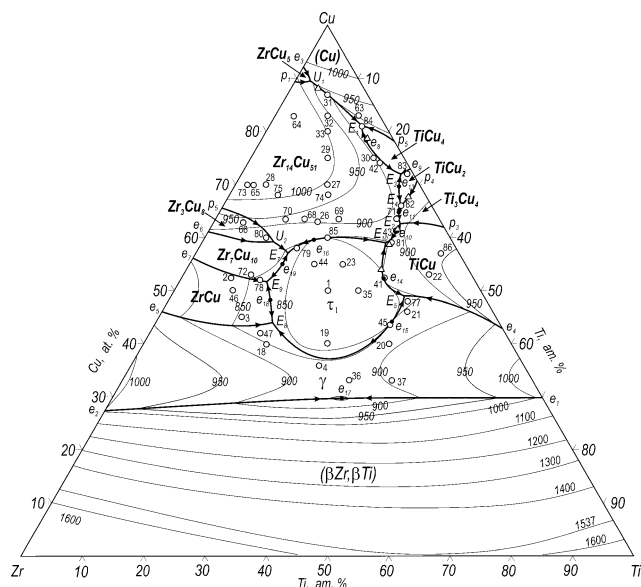


Fig. 2 Liquidus projection from this investigation: ○—composition of studied alloys, Δ—microprobe measurements of eutectic compositions.

a narrow primary field of Ti₂Cu₃, even though this compound forms in the solid state in the binary system (Fig. 1b). This result has not been confirmed by us. The primary fields of γ , τ_1 and Zr₁₄Cu₅₁ are the widest. For the τ_1 phase, this is consistent with the results of (Ref 6, 23, 24). The wide field of primary crystallization of Zr₁₄Cu₅₁ was calculated by (Ref 23, 24) and the wide primary field of γ was shown by (Ref 24).

The liquidus isotherms were constructed based on the DTA results (Table 2), and were additionally refined via the constructed vertical sections, so that each alloy was involved in at least two sections. The boundaries of the primary regions were established based on the microstructure (Fig. 3) and EPMA results (Table 3) of cast alloys.

Alloys # 4, 18, 20, 21, 47 (Fig. 3a), 77 and # 19 (Fig. 3b) are located in the fields of primary crystallization of γ and τ_1 phase, respectively, and alloy # 45 (Fig. 3c) is entirely eutectic $\gamma + \tau_1$. So, microstructures of these alloys define the position of the monovariant eutectic curve $L \leftrightarrow \gamma + \tau_1$ as it is shown in Fig. 2. The primary field of the γ -phase, thus, extends from Zr–Cu to Ti–Cu system. Inside this field the saddle point occurs at 875 °C at 38 at.% Ti. It corresponds to the minimum melting temperature of the γ -phase. From this point the liquidus temperature increases towards both Cu and Zr–Ti sides. On the monovariant curve $L \leftrightarrow \gamma + \tau_1$ occurs a flat temperature maximum at about 850 °C from which the temperature decreases towards ternary eutectics $L \leftrightarrow \gamma + \tau_1 + \text{ZrCu}$ (E₈, 828 °C) and $L \leftrightarrow \gamma + \tau_1 + \text{TiCu}$ (E₅, 848 °C). According to,^[24] the second equilibrium is of transition type $L + \gamma \leftrightarrow \tau_1 + \text{TiCu}$. In addition,^[24] calculated one minimum (at 860 °C) and two maxima (868 and 864 °C) for the equilibrium $L \leftrightarrow \gamma + \tau_1$.

In contrast to alloy # 47 (Fig. 3a) with primary γ -phase ZrCu crystallizes first in alloy # 3 (Fig. 3d). So, the monovariant curve $L \leftrightarrow \gamma + \text{ZrCu}$ passes between the compositions of these alloys.

The monovariant eutectic curve $L \leftrightarrow \text{ZrCu} + \text{Zr}_7\text{Cu}_{10}$ limits the primary region of ZrCu on the copper-rich side. It passes between the compositions of alloys # 2 and 72 (Fig. 3e, f), where ZrCu and Zr₇Cu₁₀ are the primary phases, respectively. It is important that in both samples, after the crystallization of the primary phases, the γ -phase crystallizes. In both samples, this is a nonequilibrium phase. Its appearance might be associated with similar thermodynamic stability of Zr–Cu intermetallics similar enthalpies of formation of solid phases and enthalpies of mixing of the melt.^[32] Among these phases ZrCu is less stable than Zr₂Cu (γ) and Zr₇Cu₁₀. Equilibrium crystallization of alloy # 72 would end in ternary eutectic $L \leftrightarrow \text{ZrCu} + \text{Zr}_7\text{Cu}_{10} + \tau_1$ at 826 °C.

Primary Zr₃Cu₈ phase in alloy # 80 limits the primary region of Zr₇Cu₁₀ on the copper rich side. The monovariant

Table 2 Liquidus and solidus temperatures of Zr-Ti-Cu alloys

#	Sample	Heat treatment	Temperature, °C		Other effects	
			Liquidus	Solidus	Temperature, °C	Interpretation
1	2	3	4	5	6	7
1	Zr ₂₅ Ti ₂₅ Cu ₅₀	Cast	862	848		
		Annealed	868	848		
2	Zr ₄₀ Ti _{7.7} Cu _{52.3}	Annealed	865	841		
3	Zr _{41.9} Ti _{13.3} Cu _{44.8}	Cast	860	830		
		Annealed	845, 849		751, 756	$\gamma + \tau_1 + \text{ZrCu}/\gamma + \tau_1$
4	Zr _{33.7} Ti _{30.5} Cu _{35.8}	Cast	862 [880]	836		
		Annealed	863	841		
18	Zr ₄₀ Ti ₂₀ Cu ₄₀	Cast	855	830		
		Annealed	860	834		
19	Zr ₃₀ Ti ₃₀ Cu ₄₀	Annealed	864	853	836	$\tau_1/\tau_1 + \gamma$
20	Zr ₂₀ Ti ₄₀ Cu ₄₀	Cast	885	845		
		Annealed	891	849		
21	Zr ₁₄ Ti ₄₀ Cu ₄₆	Cast	885	845		
		Annealed	882	850		
22	Zr ₇ Ti ₄₀ Cu ₅₃	Cast	930	825	850?	
23	Zr ₂₀ Ti ₂₅ Cu ₅₅	Cast	860	825		
		Annealed	864			
26	Zr ₂₀ Ti ₁₇ Cu ₆₃	Cast	945	835		
27	Zr ₁₅ Ti ₁₅ Cu ₇₀	Cast	1000	826	870	$L + \text{Zr}_{14}\text{Cu}_{51}/L + \text{Zr}_{14}\text{Cu}_{51} + \text{TiCu}$
28	Zr ₂₅ Ti ₅ Cu ₇₀	Cast	1050	830		
		Annealed	1054, 1052	830, 827, 831		
29	Zr ₁₆ Ti ₇ Cu ₇₇	Annealed	1060	855		
30	Zr ₅ Ti ₂₀ Cu ₇₅	Annealed	911	863		
31	Zr _{6.5} Ti _{6.5} Cu ₈₇	Annealed	944, 940	881	856	$(\text{Cu}) + \text{Zr}_{14}\text{Cu}_{51}/(\text{Cu}) + \text{Zr}_{14}\text{Cu}_{51} + \text{TiCu}_4$
32	Zr _{8.5} Ti _{8.5} Cu ₈₃	Annealed	960	884	898	$L + \text{Zr}_{14}\text{Cu}_{51}/L + \text{Zr}_{14}\text{Cu}_{51} + \text{ZrCu}_5$
33	Zr ₁₀ Ti ₁₀ Cu ₈₀	Annealed	998	880	897	$L + \text{Zr}_{14}\text{Cu}_{51}/L + \text{Zr}_{14}\text{Cu}_{51} + (\text{Cu})$
35	Zr ₂₀ Ti ₃₀ Cu ₅₀	Annealed	871	850		
41	Zr _{14.2} Ti _{33.1} Cu _{52.7}	Cast	873	851		
		Annealed	867			
42	Zr _{4.1} Ti _{21.7} Cu _{74.2}	Annealed	877	866		
43	Zr _{8.2} Ti _{30.4} Cu _{61.4}	Cast	916	877		
44	Zr _{24.3} Ti _{20.7} Cu ₅₅	Annealed	879	840		
45	Zr _{18.1} Ti _{38.3} Cu _{43.6}	Cast	873	850		
		Annealed	877			
47	Zr _{39.9} Ti _{18.1} Cu ₄₂	Cast	843	825		
		Annealed	848	825		
63	Zr _{3.5} Ti _{13.5} Cu ₈₃	Annealed	903	879		
64	Zr ₁₄ Ti ₃ Cu ₈₃	Annealed	1069, 1068	937		
65	Zr ₂₇ Ti ₃ Cu ₇₀	Annealed	1055	870	889	$L + \text{Zr}_3\text{Cu}_8/L + \text{Zr}_3\text{Cu}_8 + \text{Zr}_7\text{Cu}_{10}$
66	Zr ₃₂ Ti ₅ Cu ₆₃	Annealed	920	865		
68	Zr ₂₂ Ti _{14.5} Cu _{63.5}	Cast	948	851		
		Annealed	947	...	827	$\text{Zr}_{14}\text{Cu}_{51} + \tau_1/\text{Zr}_{14}\text{Cu}_{51} + \tau_2$
69	Zr _{16.5} Ti ₂₀ Cu _{63.5}	Annealed	937	825	859	$L + \text{Zr}_{14}\text{Cu}_{51}/L + \text{Zr}_{14}\text{Cu}_{51} + \tau_1$
71	Zr ₇ Ti _{29.5} Cu _{63.5}	Annealed	887	870		

Table 2 continued

1	2	3	4	5	6	7
72	Zr ₃₆ Ti ₁₁ Cu ₅₃	Cast Annealed Annealed	872 858 859	827 821 824	756 755	? ?
73	Zr ₂₈ Ti ₂ Cu ₇₀	Cast Annealed	[1055]	874 868	969 923 890	L+Zr ₁₄ Cu ₅₁ /L+Zr ₁₄ Cu ₅₁ +Zr ₃ Cu ₈ L +Zr ₁₄ Cu ₅₁ +Zr ₃ Cu ₈ /L+Zr ₃ Cu ₈ L +Zr ₃ Cu ₈ /L+Zr ₃ Cu ₈ +Zr ₇ Cu ₁₀
74	Zr ₁₆ Ti ₁₆ Cu ₆₈	Annealed	972	826		
75	Zr ₂₄ Ti ₈ Cu ₆₈	Annealed	1022	831		
77	Zr ₁₃ Ti ₃₉ Cu ₄₈	Cast	870	848		
78	Zr ₃₅ Ti ₁₃ Cu ₅₂	Cast	...	834		
82	Zr ₅ Ti ₂₉ Cu ₆₆	Cast	...	857		

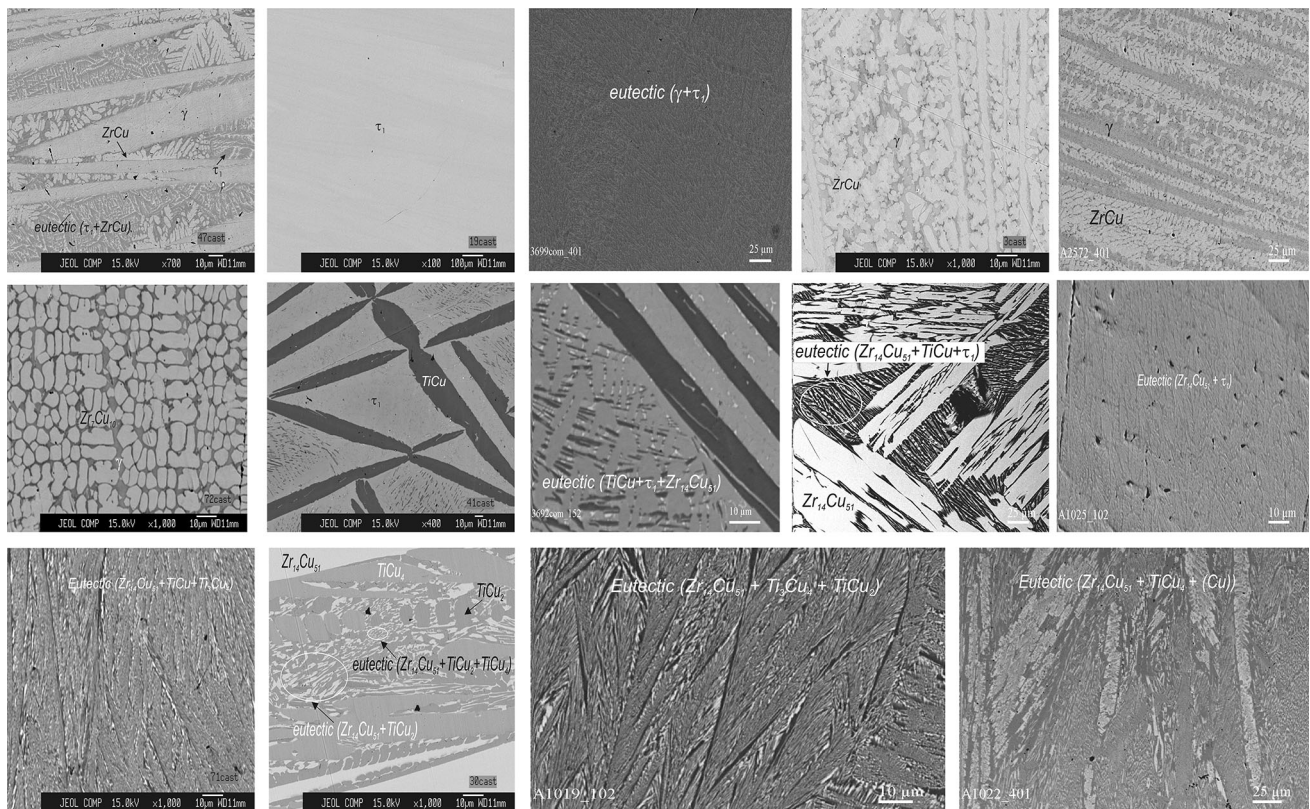


Fig. 3 Microstructures of as-cast Zr-Ti-Cu alloys: (a) Cu₄₂Ti_{18.1}Zr_{39.9}, 47cast (b) Zr₃₀Ti₃₀Cu₄₀, 19cast (c) Zr_{18.1}Ti_{38.3}Cu_{43.6}, 45cast (d) Zr_{41.9}-Ti_{13.3}Cu_{44.8}, 3cast (e) Zr₄₀Ti_{7.7}Cu_{52.3}, 2cast (f) Zr₃₆Ti₁₁Cu₅₃, 72cast (g) Zr_{14.2}Ti_{33.1}Cu_{52.7}, 41cast × 400 (h) Zr_{14.2}Ti_{33.1}Cu_{52.7}, 41cast ×

1500 (i) Zr₁₅Ti₁₅Cu₇₀, 27cast (j) Zr₂₀Ti₂₀Cu₆₀, 85cast (k) Zr₇Ti_{29.5}-Cu_{63.5}, 71cast (l) Zr₅Ti₂₀Cu₇₅, 30cast (m) Zr₅Ti₂₉Cu₆₆, 82cast (n) Zr₄Ti₁₅Cu₈₁, 84cast

curves $L \rightleftharpoons ZrCu + \tau_1$ and $L \rightleftharpoons Zr_7Cu_{10} + \tau_1$ is shown tentatively in Fig. 2.

The small amount of primary TiCu phase in alloy # 41 (Fig. 3g) allowed us to plot the monovariant curve $L \rightleftharpoons$

TiCu + τ_1 as shown in Fig. 2. The location of the curve is supported by microprobe measurements of eutectic composition in alloy # 22 (Table 3). Consideration of intergranular space at magnification × 1500 (Fig. 3h) shows the

Table 3 Crystallization pass in as-cast Zr-Ti-Cu alloys, phase composition on the solidus surface and EPMA results

N	Nominal alloy composition, at. %	Crystallization pass according to the microstructure (primary phase—in bold)	Phase composition at the solidus temperatures	Microprobe measurements, at. %				
				Phase constituent	Zr	Ti	Cu	
1	2	3	4	5	6	7	8	
2	Zr ₄₀ Ti _{17.7} Cu _{52.3}	ZrCu → γ^1	ZrCu+Zr ₇ Cu ₁₀	ZrCu	42.7	7.3	50.0	
3	Zr _{41.9} Ti _{13.3} Cu _{44.8}	ZrCu → γ	ZrCu+ γ	γ	36.0	28.3	35.7	
				ZrCu	41.6	9.1	49.3	
				γ	42.3	7.8	49.9	
				γ	46.0	20.4	33.6	
4	Zr _{33.7} Ti _{30.5} Cu _{35.8}	γ →eutectic (γ + τ_1)	γ + τ_1	τ_1	39.2	27.2	33.6	
				γ	32.3	24.7	43.0	
				γ	34.3±0.2	32.6±0.3	33.1±0.1	
18	Zr ₄₀ Ti ₂₀ Cu ₄₀	γ →eutectic (γ + τ_1)	γ +ZrCu+ τ_1	γ	46	21	33	
				γ + τ_1	35	18.5	46.5	
19	Zr ₃₀ Ti ₃₀ Cu ₄₀	τ_1	τ_1	τ_1	29.7±0.6	29.8±0.2	40.5±0.3	
20	Zr ₅₀ Ti ₄₀ Cu ₄₀	γ +eutectic (γ + τ_1)	γ + τ_1	γ	13.3	53.2	33.5	
				τ_1	24.3	30.7	45.0	
21	Zr ₁₄ Ti ₄₀ Cu ₄₆	γ →eutectic (γ + τ_1)	γ + τ_1	γ	5.6	61.0	33.4	
				τ_1	4.2	62.6	33.2	
				τ_1	18.6	30.6	50.8	
				γ + τ_1	7.1	56.3	36.6	
22	Zr ₇ Ti ₄₀ Cu ₅₃	TiCu → τ_1 →eutectic (τ_1 +Zr ₁₄ Cu ₅₁)+eutectic (TiCu+ τ_1)→eutectic (TiCu+ τ_1 +Zr ₁₄ Cu ₅₁)	TiCu+ τ_1 +Zr ₁₄ Cu ₅₁	TiCu	1.8	48.8	49.4	
				τ_1	20.0	27.8	52.2	
				τ_1 +Zr ₁₄ Cu ₅₁	19.9	2.9	77.2	
				e (TiCu+ τ_1)	14.2	31.7	54.1	

Table 3 continued

1	2	3	4	5	6	7	8
23	Zr ₂₀ Ti ₂₅ Cu ₅₅	$\tau_1 \rightarrow \{Zr_{14}Cu_{51}\}^2$	$\tau_1 + Cu_{51}Zr_{14}$	τ_1	21.0±0.2	25.8±0.1	53.2±0.2
26	Zr ₂₀ Ti ₁₇ Cu ₆₃	$Zr_{14}Cu_{51} \rightarrow \tau_1 \rightarrow \text{eutectic } (Zr_{14}Cu_{51} + \tau_1)$	$Zr_{14}Cu_{51} + \tau_1$	$Cu_{51}Zr_{14}$	20.1	9.6	70.3
				τ_1	20.2	1.9	77.9
				$Zr_{14}Cu_{51} + \tau_1$	20.5	26.7	52.8
				$e (Zr_{14}Cu_{51} + \tau_1)$	20.2	2.6	77.2
27	Zr ₁₅ Ti ₁₅ Cu ₇₀	$Zr_{14}Cu_{51} \rightarrow \text{eutectic } (Zr_{14}Cu_{51} + \tau_1 + TiCu)$	$Zr_{14}Cu_{51} + TiCu + \tau_1$	$Zr_{14}Cu_{51}$	19.8	17.9	62.3
				TiCu	18.7±0.2	3.3±0.3	78.0
				$Zr_{14}Cu_{51} + TiCu$	2.4	47.9	49.7
				$E (Zr_{14}Cu_{51} + \tau_1 + TiCu)$	14.1	18.5	67.4
28	Zr ₂₅ Ti ₅ Cu ₇₀	$Zr_{14}Cu_{51} \rightarrow \tau_1 + Zr_7Cu_{10}$	$Zr_{14}Cu_{51} + \tau_1 + Zr_7Cu_{10}$	$Zr_{14}Cu_{51}$	10.2	31.2	58.6
				τ_1	21.4	0.5	78.1
				Zr_7Cu_{10}	24.0	22.6	53.4
				$Zr_{14}Cu_{51}$	32.4	8.9	58.7
29	Zr _{12.5} Ti _{12.5} Cu ₇₅	$Zr_{14}Cu_{51} \rightarrow TiCu_2 \rightarrow Ti_3Cu_4 \rightarrow \text{eutectic } (Zr_{14}Cu_{51} + TiCu_2 + Ti_3Cu_4)$	$Zr_{14}Cu_{51} + Ti_3Cu_4 + TiCu_2$	$Zr_{14}Cu_{51}$ (center)	19.6	2.4	78.0
				$Zr_{14}Cu_{51}$ (periphery)	14.6	8.0	77.4
				TiCu ₂	1.0	31.2	67.8
				TiCu ₂ +Ti ₃ Cu ₄	0.9	36.2	62.9
				$Zr_{14}Cu_{51} + TiCu_2$	3.2	28.3	68.5
30	Zr ₅ Ti ₂₀ Cu ₇₅	$Zr_{14}Cu_{51} \rightarrow TiCu_4 \rightarrow TiCu_2 \rightarrow \text{eutectic } (Zr_{14}Cu_{51} + TiCu_2)$	$Zr_{14}Cu_{51} + TiCu_2 + TiCu_4$	$Zr_{14}Cu_{51}$	10.4	11.9	77.7
				TiCu ₄	1.3	20.5	78.2
				TiCu ₂	0.8	31.2	68.0
				$Zr_{14}Cu_{51} + TiCu_2$	3.5	26.3	70.2
31	Zr _{6.5} Ti _{6.5} Cu ₈₇ (Zr _{7.3} Ti _{5.1} Cu _{87.6}) ³	eutectic (Zr ₁₄ Cu ₅₁ +(Cu))	$Zr_{14}Cu_{51} + TiCu_4 + (Cu)$	$Zr_{14}Cu_{51}$ (center)	15.5	5.9	78.6
				TiCu ₄	1.1	20.5	78.4
				$e (Zr_{14}Cu_{51} + (Cu))$	7.4	4.7	87.9

Table 3 continued

1	2	3	4	5	6	7	8
32	Zr _{18.5} Ti _{18.5} Cu ₈₃	Zr ₁₄ Cu ₅₁ → (Cu) + TiCu ₄ → eutectic (Zr ₁₄ Cu ₅₁ + (Cu))	Zr ₁₄ Cu ₅₁ + TiCu ₄ + (Cu)	Zr ₁₄ Cu ₅₁ (center) TiCu ₄ (Cu) Zr ₁₄ Cu ₅₁ + (Cu)	16.0 1.6 0.1 7.5	5.7 19.6 4.5 6.4	78.3 78.8 95.4 86.1
33	Zr ₁₀ Ti ₁₀ Cu ₈₀	Zr ₁₄ Cu ₅₁ → TiCu ₄ + (Cu) → eutectic (Zr ₁₄ Cu ₅₁ + TiCu ₄)	Zr ₁₄ Cu ₅₁ + TiCu ₄ + (Cu)	Zr ₁₄ Cu ₅₁ (center) Zr ₁₄ Cu ₅₁ (periphery) TiCu ₄ (Cu) e (Zr ₁₄ Cu ₅₁ + TiCu ₄)	17.2 ± 0.2 11.5 1.7 0.1 3.7	4.6 10.2 19.3 8.2 17.0	78.1 ± 0.1 78.3 79.0 91.7 79.3
41	Zr _{14.2} Ti _{33.1} Cu _{52.7}	TiCu → τ ₁ → eutectic (τ ₁ + TiCu + Zr ₁₄ Cu ₅₁)	τ ₁ + TiCu	τ ₁ τ ₁ + TiCu	18.4 ± 0.2 4.4	28.7 ± 0.4 46.3	52.9 ± 0.6 49.3
42	Zr _{4.1} Ti _{21.7} Cu _{74.2}	Zr ₁₄ Cu ₅₁ → TiCu ₄ → TiCu ₂ → eutectic (TiCu ₄ + TiCu ₂) → eutectic (Zr ₁₄ Cu ₅₁ + TiCu ₂)	Zr ₁₄ Cu ₅₁ + TiCu ₂ + TiCu ₄	Zr ₁₄ Cu ₅₁ TiCu ₄ TiCu ₄ + TiCu ₂ Zr ₁₄ Cu ₅₁ + TiCu ₂ TiCu	14.7 10.3 1.4 0.7 4.5	33.3 12.1 20.3 31.4 24.1	52.0 77.6 78.3 67.9 71.4
43	Zr _{8.2} Ti _{30.4} Cu _{61.4}	eutectic (TiCu + Zr ₁₄ Cu ₅₁)	TiCu + Zr ₁₄ Cu ₅₁	TiCu TiCu + Zr ₁₄ Cu ₅₁ e (TiCu + Zr ₁₄ Cu ₅₁)	1.7 12.8 7.7	46.9 16.3 31.6	51.4 70.9 60.7
44	Zr _{24.3} Ti _{20.7} Cu ₅₅	τ ₁ → eutectic (τ ₁ + Zr ₁₄ Cu ₅₁)	τ ₁ + Zr ₁₄ Cu ₅₁	τ ₁ τ ₁ + Zr ₁₄ Cu ₅₁	8.1 24.1 ± 0.3 23.6	31.0 22.5 14.2	60.9 53.4 ± 0.2 62.2
45	Zr _{18.1} Ti _{38.3} Cu _{43.6}	eutectic (γ + τ ₁)	γ + τ ₁	τ ₁ in e (γ + τ ₁) γ + τ ₁	24.7 21.2 18.2	20.9 31.0 38.8	54.4 47.8 43.0

Table 3 continued

1	2	3	4	5	6	7	8
46	Zr _{40.5} Ti _{9.5} Cu ₅₀ (Zr _{40.5} Ti _{9.5} Cu ₅₀)	ZrCu	ZrCu	ZrCu (center) ZrCu (periphery)	41.9±0.1 38.1±0.1	7.0±0.5 11.6±0.1	50.2±0.3 50.3±0.2
47	Cu ₄₂ Ti ₁₈ Zr _{39.9}	$\gamma \rightarrow \text{ZrCu} \rightarrow \text{eutectic } (\gamma + \text{ZrCu}) + \text{eutectic } (\tau_1 + \text{ZrCu}) \rightarrow \text{eutectic } (\gamma + \text{ZrCu} + \tau_1)$	$\gamma + \text{CuZr} + \tau_1$	γ ZrCu	46.0 38.6±0.3	19.6 11.7±0.3	34.4 49.7
63	Zr _{3.5} Ti _{13.5} Cu ₈₃	$(\text{Cu}) \rightarrow \text{Zr}_{14}\text{Cu}_{51} + \text{TiCu}_4 \rightarrow \text{eutectic } (\text{Zr}_{14}\text{Cu}_{51} + \text{TiCu}_4)$	Zr ₁₄ Cu ₅₁ + TiCu ₄ + (Cu)	ZrCu + τ_1 (Cu) TiCu ₄ Zr ₁₄ Cu ₅₁ + TiCu ₄	0.1 1.7 9.8	6.5 19.6 11.5	93.4 78.7 78.7
64	Zr ₁₄ Ti ₁₃ Cu ₈₃	$\text{Zr}_{14}\text{Cu}_{51} \rightarrow \text{eutectic } (\text{Zr}_{14}\text{Cu}_{51} + (\text{Cu}))$	Zr ₁₄ Cu ₅₁ + (Cu)	Zr ₁₄ Cu ₅₁ (Cu) in eutectic Zr ₁₄ Cu ₅₁ + (Cu)	9.6 2.9 20.0	11.8 19.1 1.4±0.1	78.6 78.0 78.6±0.1
65	Zr ₂₇ Ti ₁₃ Cu ₇₀	$\text{Zr}_{14}\text{Cu}_{51} \rightarrow \text{Zr}_3\text{Cu}_8 + \text{Zr}_7\text{Cu}_{10}$	Zr ₁₄ Cu ₅₁ + Zr ₇ Cu ₁₀	Zr ₁₄ Cu ₅₁ Zr ₇ Cu ₁₀	21.6 34.9	0.3 6.2	78.1 58.9
66	Zr ₃₂ Ti ₁₃ Cu ₆₃	$\text{Zr}_3\text{Cu}_8 \rightarrow \text{Zr}_7\text{Cu}_{10}$	Zr ₃ Cu ₈ + Zr ₇ Cu ₁₀	Zr ₃ Cu ₈ Zr ₇ Cu ₁₀	26.3 34.8	1.6 6.4	72.1 58.8±0.1
68	Zr ₂₂ Ti _{14.5} Cu _{63.5}	$\text{Zr}_{14}\text{Cu}_{51} \rightarrow \text{eutectic } (\text{Zr}_{14}\text{Cu}_{51} + \tau_1)$	Zr ₁₄ Cu ₅₁ + τ_1	Zr ₁₄ Cu ₅₁ τ_1 Zr ₁₄ Cu ₅₁ + τ_1	20.6 23.7±0.2 21.3	1.4 23.1±0.2 4.8	78.0 53.2±0.2 73.9
69	Zr _{16.5} Ti ₂₀ Cu _{63.5}	$\text{Zr}_{14}\text{Cu}_{51} \rightarrow \text{eutectic } (\text{Zr}_{14}\text{Cu}_{51} + \tau_1) \rightarrow \text{eutectic } (\text{Zr}_{14}\text{Cu}_{51} + \tau_1 + \text{TiCu})$	Zr ₁₄ Cu ₅₁ + τ_1 + TiCu	Zr ₁₄ Cu ₅₁ τ_1 TiCu + τ_1	21.4 22.3 21.3	5.0 15 12.4	73.6 62.7 66.3
71	Zr ₇ Ti _{29.5} Cu _{63.5}	eutectic (Zr ₁₄ Cu ₅₁ + TiCu + Ti ₃ Cu ₄)	Zr ₁₄ Cu ₅₁ + TiCu + Ti ₃ Cu ₄	E (Zr ₁₄ Cu ₅₁ + TiCu + Ti ₃ Cu ₄)	6.9±0.1	30.4±0.1	62.6±0.1
72	Zr ₃₆ Ti ₁₁ Cu ₅₃	$\text{Zr}_7\text{Cu}_{10} \rightarrow \gamma$	Zr ₇ Cu ₁₀ + τ_1 + ZrCu	Zr ₇ Cu ₁₀ γ	35.2±0.2 42.4±0.2	6.1 23.5±0.2	58.7±0.2 33.9
73	Zr ₂₈ Ti ₂ Cu ₇₀	$\text{Zr}_{14}\text{Cu}_{51} \rightarrow \text{Zr}_3\text{Cu}_8 + \text{Zr}_7\text{Cu}_{10}$	Zr ₁₄ Cu ₅₁ + Zr ₃ Cu ₈ + Zr ₇ Cu ₁₀	Zr ₁₄ Cu ₅₁ Zr ₇ Cu ₁₀	21.4 37.7±0.1	0.2 3.3±0.1	78.4 59.0

Table 3 continued

1	2	3	4	5	6	7	8
74	Zr ₁₆ Ti ₁₆ Cu ₆₈	Zr₁₄Cu₅₁ → eutectic (Zr ₁₄ Cu ₅₁ + τ ₁ + TiCu)	Zr ₁₄ Cu ₅₁ + τ ₁ + TiCu	Zr ₁₄ Cu ₅₁ TiCu + τ ₁	19.7 ± 0.2 3.2	2.8 47.2	77.5 ± 0.2 49.6
75	Zr ₂₄ Ti ₈ Cu ₆₈	Zr₁₄Cu₅₁ → eutectic (Zr ₇ Cu ₁₀ + τ ₁)	Zr ₁₄ Cu ₅₁ + Zr ₇ Cu ₁₀ + τ ₁	Zr ₁₄ Cu ₅₁ Zr ₇ Cu ₁₀ + τ ₁	21.3 30.5	0.9 11.5	77.8 58.0
					28.2	16.8	55.0

Bold indicates the primary phases

¹In *Italic* nonequilibrium phases are shown.

²In { } traces of the phase are shown.

³In () the composition of the samples according to SEM measurements are shown.

presence of small amount of ternary eutectic TiCu + τ₁ + Zr₁₄Cu₅₁, which indicates the composition of the eutectic melt following the monovariant curve $L \rightleftharpoons \text{TiCu} + \tau_1$ towards the ternary eutectic. The phases in it are well distinguished by the color intensity: TiCu-black, τ₁-grey, Zr₁₄Cu₅₁-white. The composition of the ternary eutectic liquid agrees well with the relative amounts of the phases in eutectic structure. It was determined from EPMA data of alloy # 27 (Fig. 3i, Table 3). The appropriate point is plotted in Fig. 2. The temperature was established as 825 °C as an average temperature of all alloys from the TiCu + τ₁ + Zr₁₄Cu₅₁ three-phase region (Table 2).

Eutectic structure (Zr₁₄Cu₅₁ + τ₁) of alloys # 79, 85 (Fig. 3j) allowed to separate the fields of primary crystallization of Zr₁₄Cu₅₁ and τ₁ and, thus, to plot the monovariant eutectic curve $L \rightleftharpoons \text{Zr}_{14}\text{Cu}_{51} + \tau_1$.

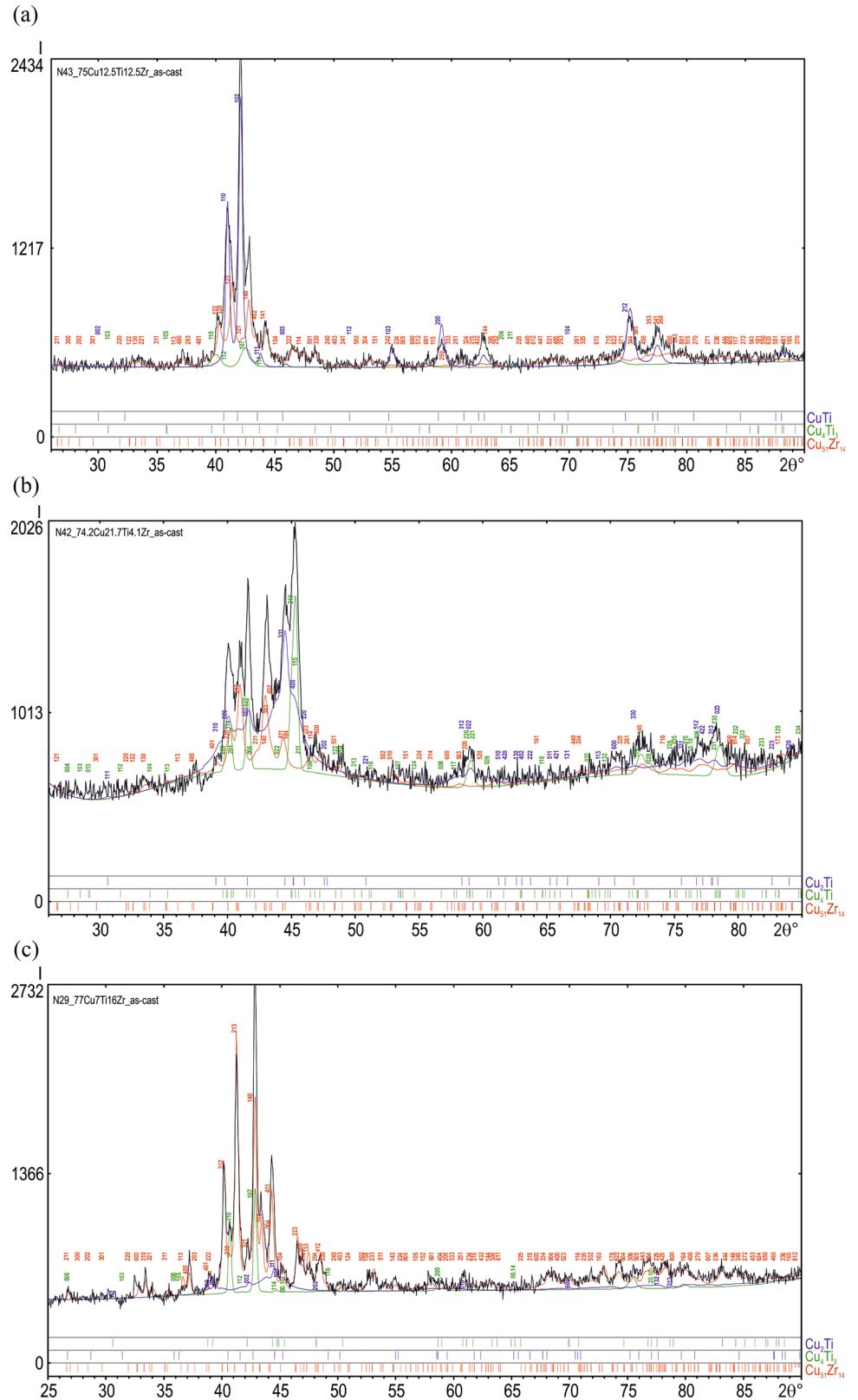
As a result of the above discussion, the region of primary crystallization of the τ₁ phase was plotted. It is wide and located in the center of the system. The region is limited by the monovariant eutectic curves $L \rightleftharpoons \gamma + \tau_1$, $L \rightleftharpoons \text{ZrCu} + \tau_1$, $L \rightleftharpoons \text{Zr}_7\text{Cu}_{10} + \tau_1$, $L \rightleftharpoons \text{Zr}_{14}\text{Cu}_{51} + \tau_1$ and $L \rightleftharpoons \text{TiCu} + \tau_1$, each of which ends in a ternary eutectic. Consequently, each of these equilibria has a temperature maximum.

The field of the primary crystallization of Zr₁₄Cu₅₁ is also wide. It is limited by the following monovariant curves: $L + \text{Zr}_{14}\text{Cu}_{51} \rightleftharpoons \text{Zr}_3\text{Cu}_8$, $L \rightleftharpoons \text{Zr}_7\text{Cu}_{10} + \text{Zr}_{14}\text{Cu}_{51}$, $L \rightleftharpoons \text{Zr}_{14}\text{Cu}_{51} + \tau_1$, $L \rightleftharpoons \text{Zr}_{14}\text{Cu}_{51} + \text{TiCu}$, $L \rightleftharpoons \text{Zr}_{14}\text{Cu}_{51} + \text{TiCu}$, $L \rightleftharpoons \text{Zr}_{14}\text{Cu}_{51} + \text{Ti}_3\text{Cu}_4$, $L \rightleftharpoons \text{Zr}_{14}\text{Cu}_{51} + \text{TiCu}_2$, $L \rightleftharpoons \text{Zr}_{14}\text{Cu}_{51} + \text{TiCu}_4$, $L \rightleftharpoons \text{Zr}_{14}\text{Cu}_{51} + (\text{Cu})$ and $L + \text{Zr}_{14}\text{Cu}_{51} \rightleftharpoons \text{ZrCu}_5$. Location of the curve $L \rightleftharpoons \text{Zr}_{14}\text{Cu}_{51} + \tau_1$ was discussed above. Other equilibria are considered below.

Alloys # 43 and 71 (Fig. 3k) are close in composition and have entirely eutectic microstructures. Measurements of eutectic compositions (Table 3) showed their correspondence to the compositions of the alloys. In both alloys, three phases in eutectic are visible. According to XRD pattern of sample # 43 (Fig. 4a), these phases are Zr₁₄Cu₅₁, TiCu and Ti₃Cu₄. However, the grains of Ti₃Cu₄ were too small to measure its composition with EPMA. Considering that the solidus temperature in sample # 43 is somewhat higher than in sample # 71 (877 and 870 °C, respectively, Table 2), the eutectic in alloy # 71 was assigned to the ternary eutectic $L \rightleftharpoons \text{Zr}_{14}\text{Cu}_{51} + \text{TiCu} + \text{Ti}_3\text{Cu}_4$, and the eutectic in sample # 43 is $L \rightleftharpoons \text{Zr}_{14}\text{Cu}_{51} + \text{TiCu}$. The presence of small amount of the Ti₃Cu₄ phase in the eutectic of alloy # 43 can be explained by the change in the composition of the melt towards the ternary eutectic during crystallization.

Crystallization in alloys # 30, (Fig. 3l) and 42 seems to be essentially non-equilibrium. This conclusion is based on the observation of three phases in the microstructure that appear to be primary. This might be related to the cooling

Fig. 4 XRD patterns of as-cast Zr-Ti-Cu alloys:
 (a) $Zr_{8.2}Ti_{30.4}Cu_{61.4}$, 43cast
 (b) $Zr_{4.1}Ti_{21.7}Cu_{74.2}$, 42cast
 (c) $Zr_{12.5}Ti_{12.5}Cu_{75}$, 29cast



rate in the arc furnace. Thus, at the initial stage of cooling, when the cooling rate is high, the melt can be enriched in other components, up to overenrichment compared to the

equilibrium melt. In addition, at this stage, the release of heat may be greater than during equilibrium crystallization, which may lead to some increase in temperature and a

Table 4 Crystallographic characteristics of intermediate phases of Zr-Ti-Cu system

Phase 1	Crystal structure 2	Lattice parameters, Å 3	Remarks 4	Reference 5
Cu	cF4–Fm-3 m Cu	a=3.6146 a=3.617±0.003	at 25 °C Zr _{8.5} Ti _{8.5} Cu ₈₃ , #32, as-cast	(Ref 35) Th.w.
ZrCu ₅	cF24–F-43 m AuBe ₅	a=6.870		(Ref 36)
Zr ₁₄ Cu ₅₁	hP68–P6/m Gd ₁₄ Ag ₅₁	a=11.2444 c=8.2815 a=11.231±0.002 c=8.272±0.002 a=11.186±0.004 c=8.213±0.006 a=11.199±0.003 c=8.230±0.004 a=11.117±0.008 c=8.234±0.006 a=11.176±0.004 c=8.176±0.005 a=11.165±0.006 c=8.15±0.01	Zr _{21.5} Cu _{78.5} , as-cast Zr _{8.2} Ti _{30.4} Cu _{61.4} , #43, as-cast Zr ₁₅ Ti ₁₅ Cu ₇₀ , #27, as-cast Zr _{4.1} Ti _{21.7} Cu _{74.2} , #42, as-cast Zr _{12.5} Ti _{12.5} Cu ₇₅ , #29, as-cast Zr ₁₀ Ti ₁₀ Cu ₈₀ , #33, as-cast	(Ref 37) Th.w. Th.w. Th.w. Th.w. Th.w. Th.w.
Zr ₃ Cu ₈	oP44–Pnma Hf ₃ Cu ₈	a=7.8693 b=8.1547 c=9.9848		(Ref 37)
Zr ₇ Cu ₁₀	oC68–C2ca Zr ₇ Ni ₁₀	a=12.6729 b=9.3163 c=9.3466 a=12.656±0.006 b=9.309±0.004 c=9.342±0.004	Zr _{41.2} Cu _{58.8} , as-cast	(Ref 36) Th.w.
ZrCu	cP2–Pm-3 m CsCl	a=3.2587 a=3.228±0.001	Zr _{40.5} Ti _{9.5} Cu ₅₀ , #46, as-cast	(Ref 36) Th.w.
γ, Zr ₂ Cu	tI6–I4/mmm MoSi ₂	a=3.2204 c=11.832 a=3.221±0.004 c=11.195±0.009	Zr _{66.7} Cu _{33.3} , as-cast	(Ref 36) Th.w.
TiCu ₄	oP20–Pnma ZrAu ₂	a=4.525 b=4.341 c=12.95 a=4.535±0.004 b=4.350±0.003 c=12.948±0.008 a=4.536±0.004 b=4.354±0.007 c=12.957±0.009	Zr _{4.1} Ti _{21.7} Cu _{74.2} , #42, as-cast Zr ₁₀ Ti ₁₀ Cu ₈₀ , #33, as-cast	(Ref 37) Th.w. Th.w.
TiCu ₂	oC12–Cmm2 Au ₂ V	a=4.363 b=7.977 c=4.47 a=8.002±0.008 b=4.512±0.006 c=4.351±0.006	Zr _{4.1} Ti _{21.7} Cu _{74.2} , #42, as-cast	(Ref 37) Th.w.
Ti ₂ Cu ₃	tP10–P4/nmm Ti ₂ Cu ₃	a=3.13 c=13.95		(Ref 37)
Ti ₃ Cu ₄	tI14–I4/mmm Ti ₃ Cu ₄	a=3.130 c=19.940 a=3.132±0.003 c=20.050±0.02	Zr _{12.5} Ti _{12.5} Cu ₇₅ , #29, as-cast	(Ref 37) Th.w.
TiCu	tP4–P4/nmm TiCu	a=3.125 c=5.915 a=3.118±0.002 c=5.907±0.003 a=3.123±0.002 c=5.930±0.005 a=3.122±0.002 c=5.943±0.004 a=3.130±0.002 c=5.941±0.004	Ti ₅₀ Cu ₅₀ , as-cast Zr _{8.2} Ti _{30.4} Cu _{61.4} , #43, as-cast Zr ₁₅ Ti ₁₅ Cu ₇₀ , #27, as-cast Zr ₂₀ Ti ₂₅ Cu ₅₅ , #23, ann. 820 °C/10 h	(Ref 37) Th.w. Th.w. Th.w. Th.w.
γ, CuTi ₂	tI6–I4/mmm MoSi ₂	a=2.953 c=10.734		(Ref 36)
γ, Cu(Zr, Ti) ₂	tI6–I4/mmm MoSi ₂	a=3.156±0.005 c=11.02±0.02 a=2.974±0.002 c=10.770±0.01	Zr ₄₀ Ti ₂₀ Cu ₄₀ , #18, as-cast Zr _{18.1} Ti _{38.3} Cu _{43.6} , #45, as-cast	Th.w. Th.w.
τ ₁ , ZrTiCu ₂	hP12–P6 ₃ /mmc MgZn ₂	a=5.105 c=8.231 a=5.1491(3) c=8.2421(8) a=5.143 c=8.231 a=5.1507(3) c=8.2441(4) a=5.112±0.002 c=8.189±0.003 a=5.197±0.003 c=8.366±0.006 a=5.136±0.002 c=8.241±0.006 a=5.1775(3) c=8.3673(9) a=5.090±0.002 c=8.150±0.006 a=5.092±0.003 c=8.159±0.006	Zr ₂₅ Ti ₂₅ Cu ₅₀ , #1, as-cast Zr _{24.8} Ti _{23.4} Cu _{51.8} , as-cast Zr ₂₀ Ti ₃₀ Cu ₅₀ , #35, as-cast Zr _{39.9} Ti _{18.1} Cu ₄₂ , #47, as-cast Zr _{18.1} Ti _{38.3} Cu _{43.6} , #45, as-cast Zr _{27.2} Ti _{27.8} Cu ₄₅ , 800 °C Zr _{14.2} Ti _{33.1} Cu _{52.7} , #41, as-cast Zr ₇ Ti ₄₀ Cu ₅₃ , #22, as-cast	(Ref 38) (Ref 27) Th.w. Th.w. Th.w. Th.w. Th.w. Th.w. Th.w. Th.w. Th.w. Th.w.

Table 4 continued

Phase 1	Crystal structure 2	Lattice parameters, Å 3	Remarks 4	Reference 5
		a=5.122±0.003 c=8.241±0.008	Zr ₂₀ Ti ₂₅ Cu ₅₅ , #23, ann. 820 °C/10 h	Th.w.
		a=5.097±0.002 c=8.179±0.005	Zr ₂₀ Ti ₂₀ Cu ₆₀ , #85, as-cast	Th.w.
τ ₂ , Zr ₂₂ Ti _{14.5} Cu _{63.5}	Hexagonal	a=12.000 c=9.800		(Ref 21)

change in the composition of the melt. As the furnace cools, the cooling rate decreases and the sample approaches equilibrium. This leads to processes that are impossible in equilibrium crystallization.

So, possible explanation of the microstructure (Fig. 3l) can be as follows. Alloys # 30 and 42 have a small amount of the primary Zr₁₄Cu₅₁-based phase (white grains). During its crystallization, the melt becomes depleted in zirconium and its composition falls into the region of primary crystallization of TiCu₄, which crystallizes as large grey grains. Since the composition of both alloys under consideration is close to the monovariant eutectic L ⇌ Zr₁₄Cu₅₁ + TiCu₄, this first non-equilibrium step is quite justified. During the crystallization of TiCu₄, the melt becomes depleted in copper and its composition enters the region of primary crystallization of TiCu₂ (dark-grey grains). Based on the microstructure (Fig. 3l), the process ends with the crystallization of the eutectic L ⇌ Zr₁₄Cu₅₁ + TiCu₂ + TiCu₄. These three phases are identified in the XRD patterns (Fig. 4b). Alloys # 82 and 84 (Fig. 3m, n) are entirely eutectic Zr₁₄Cu₅₁ + Ti₃Cu₄ + TiCu₂ and Zr₁₄Cu₅₁ + TiCu₄ + (Cu), respectively. The XRD pattern of alloy # 29 (Fig. 4c) confirms the phases in the first eutectic. The phases in alloy # 29 are well determined by microprobe measurements (Table 3).

The primary region of Zr₃Cu₈ was constructed based on this phase being primary in alloys # 66 and 80. The primary field of ZrCu₅ is given tentatively. The region of the TiCu₂ phase is plotted due to the location of the eutectic E₄ and primary TiCu₂ in sample # 83.

Thus, most invariant points of the melt in four-phase equilibria are of eutectic type. The temperatures of these equilibria with participation of τ₁ phase are very close and vary within 20 °C. The compositions of ternary eutectics that were not experimentally established are derived from the intersection of the monovariant curves.

The presence of ternary eutectics necessitates the presence of maxima in temperatures of three-phase equilibria with the liquid.

As it is clear from the above discussion, the crystallization paths in many samples is rather complex. It is shown in Table 3 for each sample based on the microstructures.

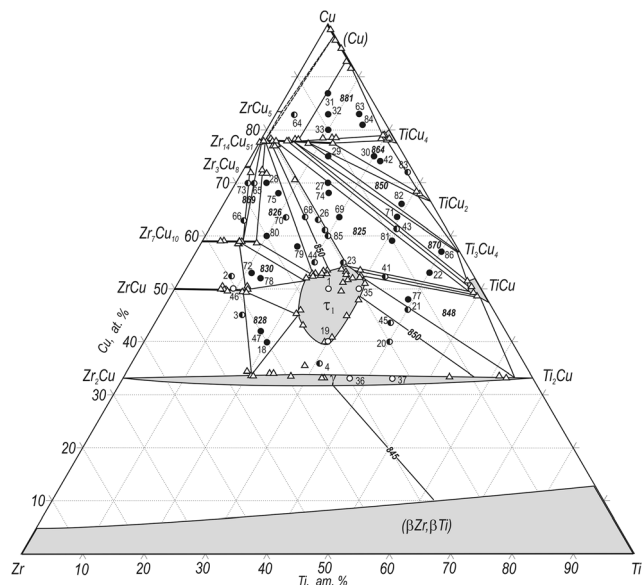


Fig. 5 Solidus projection from this investigation: ○—single-phase sample, ●—two-phase sample, ●—three-phase sample, Δ—microprobe measurements.

4.2 Solid Phases

One of the more important features of the Zr-Ti-Cu system is the presence of the ternary Laves phase τ₁ in the center of the system with a wide homogeneity range in the temperature range from 627 to 827 °C (Table 1). At solidus temperatures it is more elongated in the direction Zr/Ti-Cu and extends from ~ 39 to 54 at.% Cu, in comparison with 42.5 to 52 at.% Cu in the range of 627 to 827 °C. Completely single-phase microstructure of as-cast sample # 19 is shown in Fig. 3(b), confirming the Cu-poor boundary of the homogeneity range. The boundaries of the homogeneity range were determined by microprobe measurements (Table 3). According to our data, the solidus temperature of the phase is about 850 °C, while the congruent point was not established. These values are in satisfactory agreement with the data of (Ref 2) and (Ref 23) who reported the melting temperature as 867 and 883 °C, respectively.

The τ₂ ternary compound (Zr₂₂Ti_{14.5}Cu_{63.5}), reported in (Ref 21) was not observed by us in as-cast samples. The phase, thus, forms in the solid state.

Phases based on $ZrCu$, Zr_7Cu_{10} and $Zr_{14}Cu_{51}$ also have extended homogeneity ranges. However, unlike τ_1 , their homogeneity ranges extend along the copper isoconcentrates, which indicates the mutual substitution of Zr and Ti atoms. Ti solubility in these phases is 11, 9 and 12 at.%, respectively. Solubility of Ti in Zr_3Cu_8 is about 1 at.%. Solubility of Ti in $ZrCu_5$ was not established. Solubility of Zr in Ti-Cu intermetallics is less than 2 at.%.

As discussed above, in samples # 2 and 72 the nonequilibrium γ -phase was observed. Nevertheless, its compositions measured by microprobe method (Table 3) were used to plot the copper-rich boundary of the homogeneity range of the phase on the solidus projection.

The crystal structures of the Zr-Ti-Cu phases are listed in Table 4.

4.3 Solidus Projection

The solidus projection of the Zr-Ti-Cu system obtained by the present investigation is shown in Fig. 5. It was plotted mainly based on the results for as-cast samples. The vertices of the three-phase regions were constructed based on the microprobe results (Table 3). In several cases, these results do not refer to individual phases, but to their mixtures in various proportions as in the case of a thin grain of the measured phase, where the underlying grain or matrix is also captured by the electron probe. A similar situation exists for the coarse eutectics, where the measured composition could not be referred to the composition of the eutectic melt, but to the gross composition of two eutectic phases. For two-phase compositions, these values lie on the tie-lines and were used to construct the solidus projection. These values are also shown in Table 3. The solidus temperatures measured in as-cast samples (Table 2) are shown in Fig. 5.

According to our results, the solidus projection of Zr-Ti-Cu system is characterized by presence of the following three-phase regions: $\gamma + \tau_1 + ZrCu$, $\tau_1 + ZrCu + Zr_7Cu_{10}$, $\tau_1 + Zr_7Cu_{10} + Zr_{14}Cu_{51}$, $Zr_7Cu_{10} + Zr_{14}Cu_{51} + Zr_3Cu_8$, $\gamma + \tau_1 +$

$TiCu$, $\tau_1 + TiCu + Zr_{14}Cu_{51}$, $TiCu + Zr_{14}Cu_{51} + Ti_3Cu_4$, $Zr_{14}Cu_{51} + Ti_3Cu_4 + TiCu_2$, $Zr_{14}Cu_{51} + TiCu_2 + TiCu_4$, $Zr_{14}Cu_{51} + TiCu_4 + (Cu)$ and $Zr_{14}Cu_{51} + (Cu) + ZrCu_5$. Among them, the triangle $Zr_{14}Cu_{51} + (Cu) + ZrCu_5$ is shown tentatively.

The composition of the $ZrCu$ and Zr_7Cu_{10} phases of the region $\tau_1 + ZrCu + Zr_7Cu_{10}$ were well established by the microprobe measurements (Table 3). The composition of the τ_1 phase could not be determined, as this phase was absent in as-cast samples because of extreme nonequilibrium crystallization. Instead, the location of this corner was determined by microprobe measurements of sample # 2, annealed at a subsolidus temperature of 820 °C, which at this temperature falls into three-phase region of interest. The microstructure of sample # 2 annealed at 820 °C is shown in Fig. 6(a), where three above phases are observed.

The character of the solidus projection plotted by us is for most features consistent with the results of thermody-

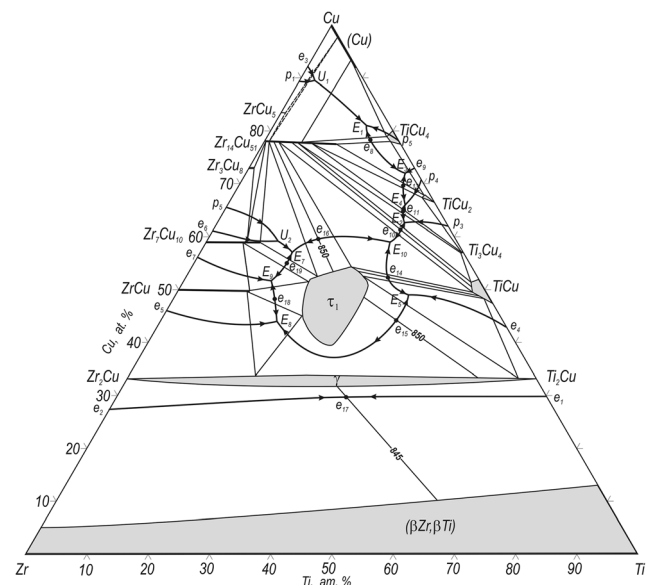


Fig. 7 Superposition of liquidus and solidus projections of the Zr-Ti-Cu system

Fig. 6 Microstructures of key alloys annealed at subsolidus temperatures:

- (a) $Zr_{40}Ti_{17.7}Cu_{52.3}$, 2cast, ann. 750 °C/736 h + 820 °C/10 h
- (b) $Zr_{20}Ti_{25}Cu_{55}$, 23cast, ann. 750 °C/736 h + 820 °C/10 h
- (c) $Zr_{16}Ti_{16}Cu_{68}$, 74cast, ann. 750 °C/736 h + 800 °C/10 h

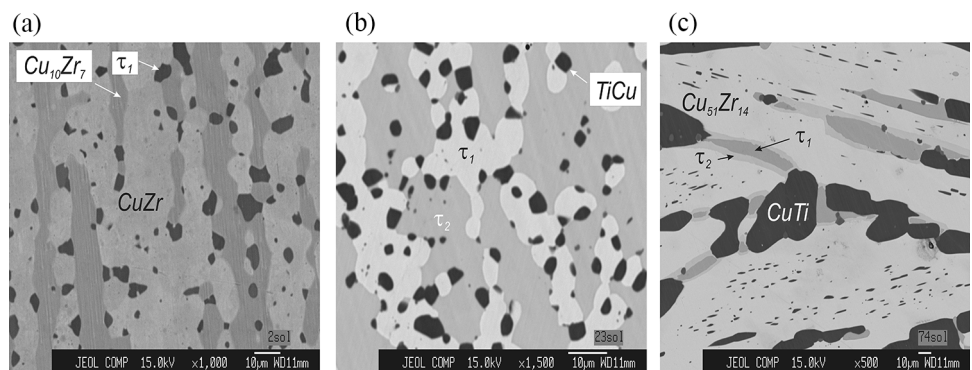


Table 5 Invariant equilibria with participation of the melt

Equilibrium	Type	Liquid composition, at. %			Temperature, °C	Reference
		Cu	Ti	Zr		
1	2	3	4	5	6	7
Four-phase equilibria						
$L + ZrCu_5 \rightleftharpoons TiCu_4 + (Cu)$	U ₃				863	(Ref 23)
$L + ZrCu_5 \rightleftharpoons TiCu_4 + Zr_{14}Cu_{51}$	U ₆				855	(Ref 23)
$L + ZrCu_5 \rightleftharpoons Zr_{14}Cu_{51} + (Cu)$	U ₁	89	3	8	954	(Ref 24)
	U₁				881 < t < 980	Th.w.
$L + (Cu) \rightleftharpoons TiCu_4 + Zr_{14}Cu_{51}$	U ₂	76.8	18.7	4.5	857	(Ref 24)
$L \rightleftharpoons Cu_4Ti + Cu_{51}Zr_{14} + (Cu)$	E₁	81	15	4	881 ± 3	Th.w.
$L + Zr_3Cu_8 \rightleftharpoons Zr_7Cu_{10} + Zr_{14}Cu_{51}$	U ₅	59.6	13.8	26.6	824	(Ref 24)
	U₂				869 ± 3	Th.w.
$L + TiCu \rightleftharpoons Zr_{14}Cu_{51} + Cu_4Ti_3$	U ₁				882	(Ref 23)
$L + TiCu + Ti_3Cu_4 \rightleftharpoons Zr_{14}Cu_{51}$	P ₁	68.2	25.5	6.3	852	(Ref 24)
$L \rightleftharpoons Zr_{14}Cu_{51} + TiCu + Ti_3Cu_4$	E₂	63	30	7	865 ± 5	Th.w.
$L \rightleftharpoons TiCu_4 + Ti_2Cu_3 + Zr_{14}Cu_{51}$	E ₂				852	(Ref 23)
	E ₂	72.0	23.3	4.7	842	(Ref 24)
$L \rightleftharpoons TiCu_4 + TiCu_2 + Zr_{14}Cu_{51}$	E₃	72.5	25.5	2	864 ± 2	Th.w.
$L + Ti_3Cu_4 \rightleftharpoons Ti_2Cu_3 + Zr_{14}Cu_{51}$	U ₇				854	(Ref 23)
	U ₄	71.3	23.8	4.9	844	(Ref 24)
$L \rightleftharpoons Ti_3Cu_4 + TiCu_2 + Zr_{14}Cu_{51}$	E₄	66	29	5	850	Th.w.
$L \rightleftharpoons \gamma (Ti_2Cu) + \tau_1 + TiCu$	E ₃	47.59	34.42	17.98	...	(Ref 6)
$L + \gamma (Ti_2Cu) \rightleftharpoons \tau_1 + TiCu$	U ₅				856	(Ref 23)
$L + \gamma \rightleftharpoons \tau_1 + TiCu$	U ₃	48.7	35.1	16.2	851	(Ref 24)
$L \rightleftharpoons \gamma + \tau_1 + TiCu$	E₅	49	38	13	848	Th.w.
$L \rightleftharpoons \tau_1 + Zr_7Cu_{10} + Zr_{14}Cu_{51}$	E ₄	58.9	16.3	24.8	814	(Ref 24)
	E₇	57	15	28	830 ± 1	Th.w.
$L \rightleftharpoons \gamma (Zr_2Cu) + \tau_1 + ZrCu$	E ₁	48.63	14.24	37.13	...	(Ref 6)
	E ₄				833	(Ref 23)
$L \rightleftharpoons \gamma + \tau_1 + ZrCu$	E ₁	45.9	14.5	39.6	850	(Ref 24)
	E₈	44	19	37	828	Th.w.
$L \rightleftharpoons \tau_1 + ZrCu + Zr_7Cu_{10}$	E ₃				839	(Ref 23)
	E ₃	53.9	11.9	34.2	835	(Ref 24)
	E₉	52	14	34	826 ± 8	Th.w.
$L \rightleftharpoons \beta + \gamma (Zr_2Cu) + \tau_1$	E ₂	43.20	17.37	39.43	...	(Ref 6)
	E ₅				827	(Ref 23)
$L + \gamma (Ti_2Cu) \rightleftharpoons \beta + \tau_1$	U ₉				835	(Ref 23)
$L \rightleftharpoons \tau_1 + TiCu + Zr_{14}Cu_{51}$	E ₁				855	(Ref 23)
	E ₅	58.2	22.4	19.4	812	(Ref 24)
	E₁₀	59	30	11	825 ± 1	Th.w.
$L + Zr_{14}Cu_{51} \rightleftharpoons Zr_3Cu_8 + \tau_1$	U ₄				861	(Ref 23)
$L + Zr_3Cu_8 \rightleftharpoons Zr_7Cu_{10} + \tau_1$	U ₈				845	(Ref 23)
Three-phase equilibria						
$L \rightleftharpoons TiCu_4 + Zr_{14}Cu_{51}$	e₈(max)				> 881	Th.w.
$L \rightleftharpoons TiCu + Zr_{14}Cu_{51}$	e₁₀(max)				> 870	Th.w.
$L \rightleftharpoons Ti_3Cu_4 + Zr_{14}Cu_{51}$	e₁₁(max)				> 870	Th.w.
$L \rightleftharpoons TiCu_2 + Zr_{14}Cu_{51}$	e₁₃(max)				> 864	Th.w.
$L \rightleftharpoons TiCu + \tau_1$	e₁₄(max)				851	Th.w.

Table 5 continued

Equilibrium	Type	Liquid composition, at. %			Temperature, °C	Reference
		Cu	Ti	Zr		
1	2	3	4	5	6	7
$l \rightleftharpoons \gamma + \tau_1$	e_{11} (max)	42.1	34.9	23.0	868	(Ref 24)
	e_{12} (max)	41.0	25.1	33.9	864	(Ref 24)
	e_{13} (min)	38.7	32.1	29.2	860	(Ref 24)
	e_{15}(max)				850	Th.w.
$l \rightleftharpoons Zr_{14}Cu_{51} + \tau_1$	e_{17} (max)	58.6	18.8	22.6	815	(Ref 24)
	e_{16}(max)				850	Th.w.
$l \rightleftharpoons \gamma + \beta$	e_{15} (min)	25.8	45.0	29.2	846	(Ref 24)
	e_{17}(min)				845	(Ref 29)
$l \rightleftharpoons Zr_7Cu_{10} + \tau_1$	e_{16} (max)	54.6	12.6	32.8	836	(Ref 24)
	e_{18}(max)				>830	Th.w.
$l \rightleftharpoons ZrCu + \tau_1$	e_{14} (max)	48.2	14.6	37.2	853	(Ref 24)
	e_{19}(max)				>828	Th.w.
$Zr_{14}Cu_{51} + \tau_1 \rightleftharpoons \tau_2$	p_7				827	Th.w.

Data obtained in this work in comparison with literature data are given in bold

dynamic modelling.^[24] However, the region with the participation of Ti-Cu intermetallics is different. According to,^[24] the Ti_2Cu_3 compound, which forms in the solid state in the binary system, appears on the solidus projection in the ternary. In our investigation Ti_2Cu_3 was not observed in as-cast samples, and, thus, does not participate in equilibria on the solidus projection. The microstructure of the sample # 30 (Fig. 3l) from the region $Zr_{14}Cu_{51} + TiCu_4 + TiCu_2$ was discussed above. The XRD pattern of sample # 42 from this phase region (Fig. 4b) confirms the presence of these three phases. As a result, in contrast to $Ti_3Cu_4 + Ti_2Cu_3 + Zr_{14}Cu_{51}$ and $Ti_2Cu_3 + TiCu_4 + Zr_{14}Cu_{51}$ regions,^[24] our investigation showed the regions $Zr_{14}Cu_{51} + Ti_3Cu_4 + TiCu_2$ and $Zr_{14}Cu_{51} + TiCu_2 + TiCu_4$ to exist on the solidus projection. Alloys # 30 are 42 are in the first region, sample # 29 is located in the second one (Fig. 4c).

Most invariant equilibria, according to the liquidus projection (Fig. 2), are of the eutectic type, which results in temperature maxima on monovariant curves, and these temperature maxima should also be present in two-phase fields of the solidus projection (Fig. 5). According to our results, most of these fields are narrow and none of the alloys are located within these. For alloys which are in two-phase regions, tie-lines are plotted according to microprobe measurements and the solidus temperatures are shown. The exact locations of the maximum temperatures for the tie-lines was established only for the regions $\gamma + \tau_1$ and $\tau_1 + Zr_{14}Cu_{51}$. As can be seen from Fig. 5, the temperature maximum for the $\gamma + \tau_1$ solidus is very flat.

4.4 Invariant Equilibria with Participation of the Melt

The superposition of the liquidus and solidus projections is shown in Fig. 7. It allows a better understanding of the processes occurring in the system during crystallization. The location of the invariant points of the liquid inside or outside the three-phase regions of the solidus projection indicates the eutectic or transition-type nature of the four-phase equilibria, respectively. Among these three equilibria are of the transition type, all others are eutectics. Invariant equilibria are listed in Table 5 in comparison with data from the literature.

As mentioned above, the temperature maxima of the monovariant curves in the liquidus projection are connected to the maxima in two-phase fields of the solidus projections. Compositions of the melts in these points are located on the maximum tie-lines of the solidus surface. At these maximum temperatures the three-phase equilibria are invariant. The coordinates of three-phase invariant equilibria are also shown in Table 5.

The sequence of the processes taking place during solidification are summarized in the Scheil reaction scheme (Fig. 8).

4.5 Solid State Equilibria

Comparison of the constructed solidus projection (Fig. 5) and isothermal section at 750 °C^[21] shows that the

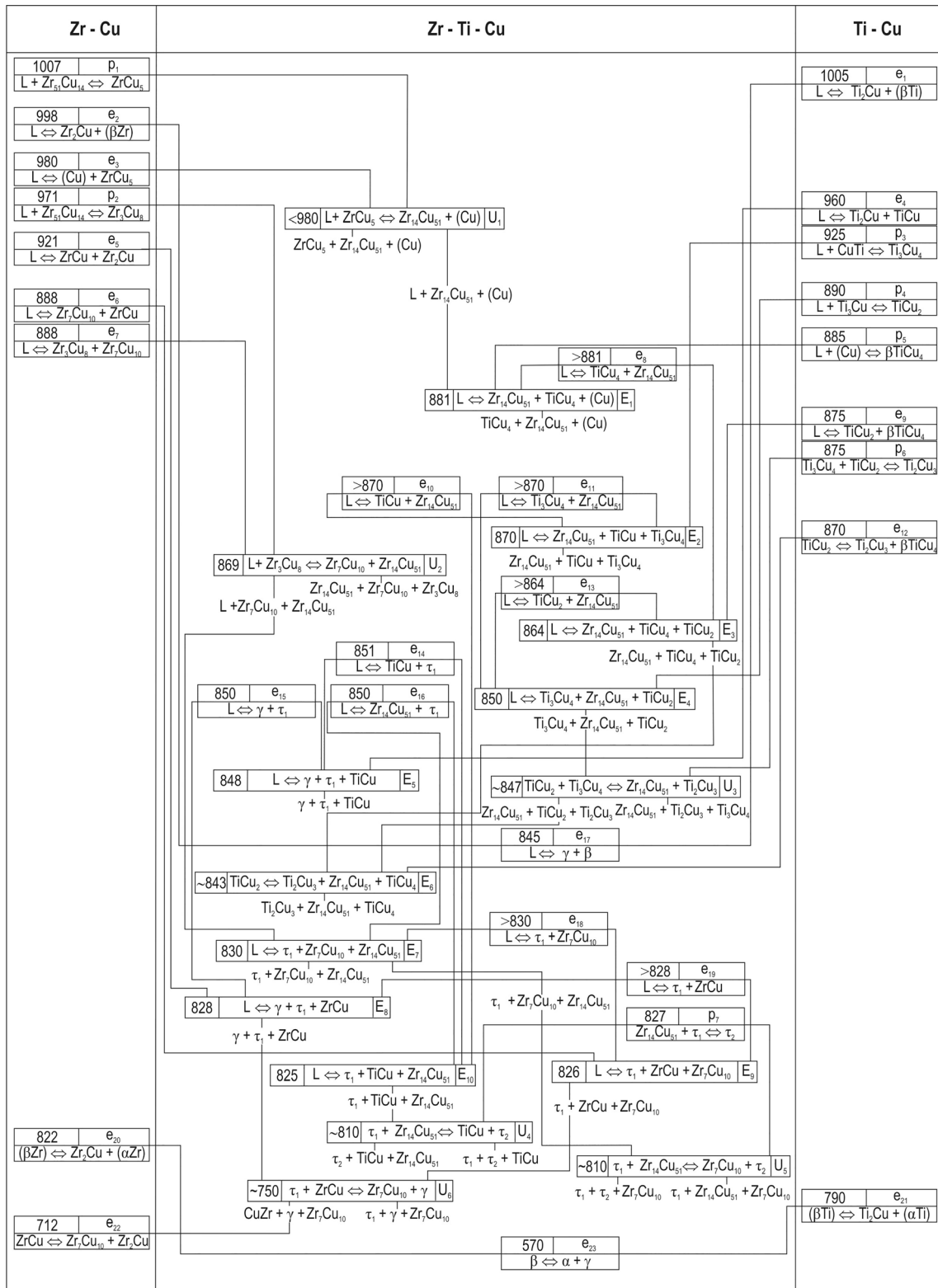


Fig. 8 Scheil reaction scheme of the Zr-Ti-Cu system

character of phase equilibria in the central part of the system is different. The principal differences are as follows:

1. The ternary compound τ_2 , which exists at 750 °C, is not present in the solidus projection. So, it forms in the solid state.

Table 6 Microprobe data for the samples annealed close to solidus temperatures after annealing at 750 °C/736 h

#	Alloy, at. %	Phase	Microprobe measurements, at. %		
			Zr 4	Ti 5	Cu 6
Annealing at 905 °C/10 h					
64	Zr ₁₄ Ti ₃ Cu ₈₃	Zr ₁₄ Cu ₅₁ (Cu)	17.6 0.0	3.6 1.7	78.8 98.3
Annealing at 855 °C/10 h					
33	Zr ₁₀ Ti ₁₀ Cu ₈₀	Zr ₁₄ Cu ₅₁ (Ti-poor) Zr ₁₄ Cu ₅₁ (Ti-rich) TiCu ₄	15.8 13.6 1.0	6.3 8.8 19.9	77.8 77.6 79.0
63	Zr _{3.5} Ti _{13.5} Cu ₈₃	Zr ₁₄ Cu ₅₁ (Cu) TiCu ₄	12.7 0.0 1.0	9.7 5.5 19.4	77.6 94.5 79.6
Annealing at 840 °C/10 h					
30	Zr ₅ Ti ₂₀ Cu ₇₅	Zr ₁₄ Cu ₅₁ TiCu ₄ Ti ₂ Cu ₃	12.4 0.9 0.2	10.3 20.5 39.4	77.3 78.6 60.4
42	Zr _{4.1} Ti _{21.7} Cu _{74.2}	Zr ₁₄ Cu ₅₁ TiCu ₄ Ti ₂ Cu ₃	13.1 0.9 0.3	10.0 20.9 39.9	76.9 78.2 59.8
65	Zr ₂₇ Ti ₃ Cu ₇₀	Zr ₇ Cu ₁₀ Zr ₁₄ Cu ₅₁	35.2 22.0	6.5 0.4	58.3 77.6
71	Zr ₇ Ti _{29.5} Cu _{63.5}	Zr ₁₄ Cu ₅₁ Ti ₃ Cu ₄ TiCu	17.1 0.7 0.5	5.3 43.4 50.0	77.6 55.9 49.5
Annealing at 820 °C/10 h					
2	Zr _{39.9} Ti _{7.8} Cu _{52.3}	ZrCu Zr ₇ Cu ₁₀ τ ₁	43.5 36.8 32.9	7.2 5.7 20.2	49.3 57.5 46.9
3	Zr _{41.9} Ti _{13.3} Cu _{44.8}	ZrCu γ τ ₁	43.7 51.6 32.6±0.3	7.0 15.1 20.2±0.2	49.1 33.3 47.2±0.2
20 ¹	Zr ₂₀ Ti ₄₀ Cu ₄₀	τ ₁ γ	24.6 13.0	29.5 53.7	45.9 33.3
21	Zr ₁₄ Ti ₄₀ Cu ₄₆	τ ₁ TiCu γ (Ti-rich)	22.6 3.2 5.8	28.5 47.8 61.2	48.9 49.0 32.9
23	Zr ₂₀ Ti ₂₅ Cu ₅₅	τ ₂ τ ₁ TiCu	21.9±0.1 23.1 3.2	14.8±0.2 26.7 47.6	63.4±0.1 50.2 49.2
41	Zr _{14.2} Ti _{33.1} Cu _{52.7}	τ ₁ TiCu τ ₂	23.0 3.3 22.3	26.9 47.2 14.6	50.1 49.5 63.1
67	Zr ₂₆ Ti ₁₄ Cu ₆₀	Zr ₇ Cu ₁₀ τ ₁ Zr ₁₄ Cu ₅₁	29.5±0.5 24.7±0.7 20.5	12.2±0.1 24.2±0.3 0.8	58.3±0.8 51.1±0.9 78.7

Table 6 continued

1	2	3	4	5	6
Annealing at 800 °C/10 h					
35 ¹	Zr ₂₀ Ti ₃₀ Cu ₅₀	τ ₁	20.8±0.2	29.0±0.2	50.2
		TiCu	3.1	47.8	49.1
37 ¹	Zr ₂₃ Ti ₄₄ Cu ₃₃	γ	21.2	45.6	33.2
45 ¹	Zr _{18.1} Ti _{38.3} Cu _{43.6}	τ ₁	22.4±0.1	29.1±0.2	48.5±0.3
		γ	6.4±0.1	60.4±0.2	33.2±0.1
69	Cu _{63.5} Ti ₂₀ Zr _{16.5}	Zr ₁₄ Cu ₅₁	21.4	1.0	77.6
		TiCu	2.4±0.1	48.3	49.3±0.2
		τ ₁	22.7	28.3	49.0
		τ ₂	21.2±0.5	14.8±0.2	64.3±0.6
74	Zr ₁₆ Ti ₁₆ Cu ₆₈	Zr ₁₄ Cu ₅₁	21.5	1.0	77.5
		TiCu	2.8	47.7	49.5
		τ ₁	22.5	27.1	50.4
		τ ₂	21.8	14.6	63.6
			20.6	14.5	64.9
75	Zr ₂₄ Ti ₈ Cu ₆₈	Zr ₇ Cu ₁₀	28.5±0.9	12.5	59±1
		τ ₁ (Zr-rich)	25.3	24.1	50.6
		τ ₁ (Zr-poor)	23.6	24.4	52.0
		τ ₂	21.4	13.8	64.4
		Zr ₁₄ Cu ₅₁	20.4	0.9	78.7

¹Annealed during 15 h.

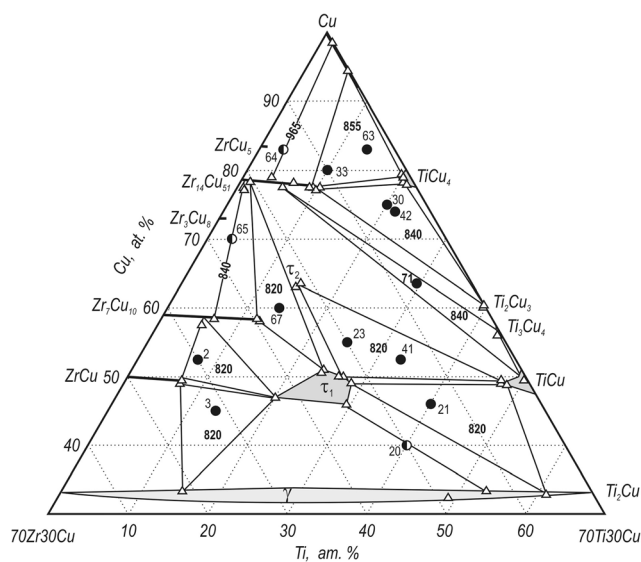


Fig. 9 Microprobe data and phase composition of the samples annealed at sub-solidus temperatures. The temperatures shown correspond to the annealing temperatures: ●—two-phase sample, ●—three-phase sample, Δ—microprobe measurements (inset: details of the equilibria with τ₁)

2. Instead of three-phase fields Zr₁₄Cu₅₁+TiCu₄+TiCu₂ and Zr₁₄Cu₅₁+TiCu₂+Ti₃Cu₄ in the solidus projection, at 750 °C there are regions Zr₁₄Cu₅₁+TiCu₄+Ti₂Cu₃

and Zr₁₄Cu₅₁+Ti₂Cu₃+Ti₃Cu₄. So, in this temperature range, a number of solid-state transformations occur involving the decomposition of TiCu₂ and the formation of Ti₂Cu₃, like the Ti-Cu system.

3. The position of the corners of three-phase regions is essentially different, resulting from changes in the homogeneity ranges of the phases, which decrease with decreasing temperature.

To address these issues, several samples previously annealed at 750 °C^[21] were annealed at sub-solidus temperatures and studied by microprobe method. Microstructures of key samples and microprobe results are shown in Fig. 6 and Table 6, respectively. These data are summarized in Fig. 9. Note that the temperatures inside the three-phase regions and on the tie-lines in Fig. 9 correspond to the annealing temperatures; therefore, the figure can be considered as superimposed fragments of isothermal sections at different temperatures.

Changes in the phase composition of samples with temperature can be seen in isopleths at 40 and 70 at.% Cu (Fig. 10).

The isopleth at 40 at.% Cu (Fig. 10a) illustrates a limited temperature range for existence of the τ₁ phase. Indeed, as-cast sample Zr₃₀Ti₃₀Cu₄₀ (# 19) is single-phase (Fig. 3b), but it contains two phases (τ₁+γ) at 800 °C and below.

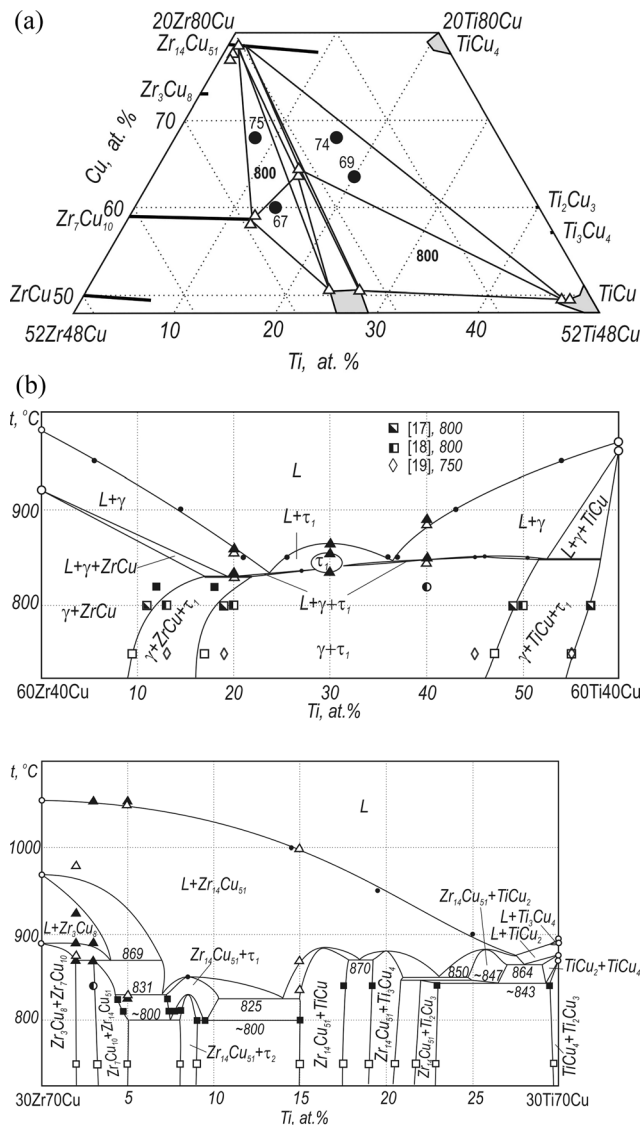


Fig. 10 Isoleth of Zr-Ti-Cu system at 40 (a) and 70 (b) at.% Cu: ○—temperature of invariant equilibria in binary systems, ●—two-phase sample, △—DTA data for as-cast samples, ▲—DTA data for annealed samples, □—boundaries of the phase fields at 750 °C^[21], ■—boundaries of the phase fields according to this investigation, ●—temperatures taken from the isotherms

In this isopleth, the phase field boundaries obtained by us for as-cast and subsolidus annealed samples are compared with the experimental results of.^[17–19, 21] As one can see, the data^[17, 18, 21] for 800 and 750 °C along the section 40 at.% Cu agree well with our results for the solidus. Along other sections, a good agreement is only observed with the^[21] data for 750 °C, which are preferred.

The isopleth at 70 at.% Cu (Fig. 10b), in addition to crystallization processes, illustrates the formation of the τ_2 phase and transformations involving Ti-Cu compounds.

The boundaries of the phase fields established by us at different temperatures (Fig. 9), and the boundaries at 750 °C^[21] are shown in the isopleth.

4.5.1 Transformations Involving Ti-Cu Compounds

The solidus projection contains the fields $Zr_{14}Cu_{51}+TiCu_4+TiCu_2$ and $Zr_{14}Cu_{51}+TiCu_2+Ti_3Cu_4$ with solidus temperatures of 864 and 850 °C, respectively. At 840 °C (Fig. 9a) none of these fields exist. Instead, the field $Zr_{14}Cu_{51}+TiCu_4+Ti_2Cu_3$ exists at 750 °C.^[21] It is natural to assume that $TiCu_2$ decomposes with the formation of Ti_2Cu_3 by eutectoid reaction, similarly to the Ti-Cu binary system. The reaction, thus, is $TiCu_2 \rightleftharpoons Zr_{14}Cu_{51}+TiCu_4+Ti_2Cu_3$, and occurs above 840 °C.

Three solid three-phase from higher temperatures form this invariant equilibrium. The equilibria $TiCu_2+TiCu_4+Ti_2Cu_3$ and $Zr_{14}Cu_{51}+TiCu_2+TiCu_4$ originate from the binary Ti-Cu system and the solidus, respectively. Another four-phase transformation should occur to form the $Zr_{14}Cu_{51}+TiCu_2+Ti_2Cu_3$ equilibrium. Taking into account the existence of the equilibrium $Zr_{14}Cu_{51}+TiCu_2+Ti_3Cu_4$ on the solidus projection and the $Zr_{14}Cu_{51}+Ti_2Cu_3+Ti_3Cu_4$ equilibrium at 750 °C, the region $Zr_{14}Cu_{51}+TiCu_2+Ti_2Cu_3$ forms by transition-type equilibrium $TiCu_2+Ti_3Cu_4 \rightleftharpoons Zr_{14}Cu_{51}+Ti_2Cu_3$. This should occur between 850 °C (solidus temperature of the $Zr_{14}Cu_{51}+TiCu_2+Ti_3Cu_4$ region) and 840 °C, and higher than the eutectoid one. Thus, between 850 and 840 °C two invariant four-phase equilibria occur, as shown in Fig. 10b.

4.5.2 Formation of the Ternary Compound τ_2

The τ_2 ternary compound was first observed in (Ref 21) at 750 °C. In our investigation it was observed in samples # 23 and 41, annealed at 820 °C (Fig. 6b, 9a). The compound, thus, forms above 820 °C. At both temperatures it is in two-phase equilibrium with $TiCu$. In sample #67 annealed at this temperature the τ_2 compound was not observed (Fig. 9a). After annealing at 800 °C sample # 75 (Table 6, Fig. 9b) contains four phases, $Zr_{14}Cu_{51}+Zr_7Cu_{10}+\tau_1+\tau_2$. Although this sample is not in equilibrium it allows to assume that between 800 and 820 °C invariant four-phase equilibrium occurs. The compositions of the phases point to the transition type equilibrium $Zr_{14}Cu_{51}+\tau_1 \rightleftharpoons Zr_7Cu_{10}+\tau_2$. Similarly, in samples # 69 and 74 annealed at 800 °C (Fig. 6c, 9b) phases $Zr_{14}Cu_{51}+TiCu+\tau_1+\tau_2$ are present indicating invariant transformation $Zr_{14}Cu_{51}+\tau_1 \rightleftharpoons TiCu+\tau_2$. One of the three-phase equilibria, $Zr_{14}Cu_{51}+\tau_1+\tau_2$, is part of both invariant reactions. Thus, the τ_2 phase forms by invariant three-phase transformation $Zr_{14}Cu_{51}+\tau_1 \rightleftharpoons \tau_2$, as shown in Fig. 10(b). The microstructure of sample #74 (Fig. 6c) shows typical peritectic formation of the τ_2

Table 7 Solid state invariant equilibria

Equilibrium	Type	Temperature, °C	Reference
$L + Ti_3Cu_4 + TiCu_2 \rightleftharpoons Ti_2Cu_3$ ¹	P ₁	874	(Ref 23)
	D ₁	877	(Ref 24)
$TiCu_2 + Ti_3Cu_4 \rightleftharpoons Zr_{14}Cu_{51} + Ti_2Cu_3$	U₃	~ 847	Th.w.
$L + Cu_2Ti \rightleftharpoons Cu_3Ti_2 + Cu_4Ti$ ¹	U ₂	869	(Ref 23)
	D ₂	864	(Ref 24)
$TiCu_2 \rightleftharpoons Ti_2Cu_3 + Zr_{14}Cu_{51} + TiCu_4$	E₆	~ 843	Th.w.
$\tau_1 + Zr_{14}Cu_{51} \rightleftharpoons TiCu + \tau_2$	U₄	~ 810	Th.w.
$\tau_1 + Zr_{14}Cu_{51} \rightleftharpoons Zr_7Cu_{10} + \tau_2$	U₅	~ 810	Th.w.
$ZrCu \rightleftharpoons \tau_1 + Zr_7Cu_{10} + \gamma$	E ₆	646	(Ref 24)
$\tau_1 + ZrCu \rightleftharpoons Zr_7Cu_{10} + \gamma$	U₆	~ 750	Th.w.
$Zr_{14}Cu_{51} + \tau_1 \rightleftharpoons \tau_2$	p₇	827	Th.w.
$\beta \rightleftharpoons \alpha + \gamma$	e ₂₃	570	(Ref 20)
$Zr_{14}Cu_{51} + Zr_7Cu_{10} \rightleftharpoons \tau_1 + Zr_3Cu_8$	D ₃	764	(Ref 24)
$Zr_{14}Cu_{51} + (Cu) \rightleftharpoons TiCu_4 + ZrCu_5$	U ₆	587	(Ref 24)
$TiCu_4 + Zr_{14}Cu_{51} \rightleftharpoons Ti_2Cu_3 + ZrCu_5$	U ₇	527	(Ref 24)
$Ti_2Cu_3 + Zr_{14}Cu_{51} \rightleftharpoons Ti_3Cu_4 + ZrCu_5$	U ₈	455	(Ref 24)
$Ti_3Cu_4 + Zr_{14}Cu_{51} \rightleftharpoons TiCu + ZrCu_5$	U ₉	303	(Ref 24)
$TiCu + \tau_1 \rightleftharpoons Zr_{14}Cu_{51} + \gamma$	U ₁₀	234	(Ref 24)
$TiCu + Zr_{14}Cu_{51} \rightleftharpoons ZrCu_5 + \gamma$	U ₁₁	93	(Ref 24)

Data obtained in this work in comparison with literature data are given in bold

¹ Equilibria are added to see the reactions with Ti-Cu compounds proposed by (Ref 23, 24).

ternary compound. The temperature of its formation was measured in sample Zr₂₂Ti_{14.5}Cu_{63.5} (# 68) as 827 °C.

The solid state transformations are listed in Table 7 and presented in the reaction scheme (Fig. 8).

5 Conclusions

As a result of a complex experimental study of phase equilibria in the Zr-Ti-Cu system, liquidus and solidus projections, the Scheil reaction scheme, and isopleths for a number of isoconcentrates were constructed for the first time. The phase equilibria are defined by the phases Zr₁₄Cu₅₁ and τ_1 , being in equilibria with all other phases on the solidus projection and having the widest fields of primary crystallization on the liquidus projection.

The τ_1 phase has wide homogeneity range, which extends from 39 to 54 at.% Cu and from 21 to 31 at.% Ti. Compounds Zr₁₄Cu₅₁ and ZrCu dissolve up to 12 at.% Ti, Zr₇Cu₁₀ dissolves 9 at.% Ti. The homogeneity ranges of these phases are located along the copper isoconcentrates. The solubility of the third component in other binary compounds does not exceed 2 at.%.

The solidus projection is characterized by presence of the following three-phase regions: $\gamma + \tau_1 + ZrCu$, $\tau_1 + ZrCu + Zr_7Cu_{10}$, $\tau_1 + Zr_7Cu_{10} + Zr_{14}Cu_{51}$, $Zr_7Cu_{10} + Zr_{14}Cu_{51} + Zr_3Cu_8$, $\gamma + \tau_1 + TiCu$, $\tau_1 + TiCu + Zr_{14}Cu_{51}$, $TiCu + Zr_{14}Cu_{51} + Ti_3Cu_4$, $Zr_{14}Cu_{51} + Ti_3Cu_4 + TiCu_2$, $Zr_{14}Cu_{51} + TiCu_2 +$

$TiCu_4$, $Zr_{14}Cu_{51} + TiCu_4 + (Cu)$ and $Zr_{14}Cu_{51} + (Cu) + ZrCu_5$. The regions $Zr_7Cu_{10} + Zr_{14}Cu_{51} + Zr_3Cu_8$ and $Zr_{14}Cu_{51} + (Cu) + ZrCu_5$ form by transition-type reactions, the rest by eutectic reactions. The temperatures of eutectic reactions are within 825-880 °C. Ten invariant three-phase eutectic equilibria occur in the system.

In contrast to the literature data, it is shown that TiCu₂ participates in equilibria with the melt and decomposes by eutectoid reaction $TiCu_2 \rightleftharpoons Zr_{14}Cu_{51} + TiCu_4 + Ti_2Cu_3$. This equilibrium and $TiCu_2 + Ti_3Cu_4 \rightleftharpoons Zr_{14}Cu_{51} + Ti_2Cu_3$ occur between 840 and 850 °C.

It is shown for the first time that the ternary compound τ_2 forms by invariant three-phase reaction $Zr_{14}Cu_{51} + \tau_1 \rightleftharpoons \tau_2$ at 827 °C.

References

1. R.F. Bunshah, D. Osterberg, E. Ence, and H. Margolin, *Further Studies on Active-Eutectoid Alloys of Titanium* U.S. Department Commerce Office Technical Services, New York, 1960, p1-73
2. Yu.K. Kovneristy and A.G. Pashkovskaya, Bulk Amorphization of Alloys in the Intermetallic-Containing System Ti-Cu-Zr, Amorphous (Glassy) Metallic Materials, *Ros. Akad. Nauk Baikov Inst. Metall.*, 1992, **1992**, p 153-157.
3. A. Peker and W.L. Johnson, A Highly Processable Metallic Glass: Zr_{41.2}Ti_{13.8}Cu_{12.5}Ni_{10.0}Be_{22.5}, *Appl. Phys. Lett.*, 1993, **63** (17), p 2342-2344.
4. A.A. Kündig, J.F. Löffler, W.L. Johnson, P.J. Uggowitzer, and P. Thiyagarajan, Influence of Decomposition on the Thermal

- Stability of Undercooled Zr-Ti-Cu-Ni-Al Alloys, *Scr. Mater.*, 2001, **44**(8–9), p 1269–1273.
5. M. Telford, The Case for Bulk Metallic Glass, *Mater. Today*, 2004, **7**(3), p 36–43.
 6. C.G. Woychik and T.B. Massalski, Phase Diagram Relationships in the System Cu-Ti-Zr, *Z. Metallkde*, 1988, **79**(3), p 149–153.
 7. A. Inoue, W. Zhang, T. Zhang, and K. Kurosaka, High-Strength Cu-based Bulk Glassy Alloys in Cu-Zr-Ti and Cu-Hf-Ti Ternary Systems, *Acta Mater.*, 2001, **49**(14), p 2645–2652.
 8. M. Kasai, J. Saida, M. Matsushita, T. Osuna, E. Matsubara, and A. Inoue, Structure and Crystallization of Rapidly Quenched Cu (Zr or Hf) Ti Alloys Containing Nanocrystalline Particles, *J. Phys. Condens. Matter*, 2002, **14**(50), p 13867–13877.
 9. D.V. Louzguine and A. Inoue, Nanocrystallization of Cu-(Zr or Hf)-Ti Metallic Glasses, *J. Mater. Res.*, 2002, **17**(08), p 2112–2120.
 10. J.Z. Jiang, B. Yang, K. Saksl, H. Franz, and N. Pryds, Crystallization of Cu₆₀Ti₂₀Zr₂₀ Metallic Glass with and Without Pressure, *J. Mater. Res.*, 2003, **18**(04), p 895–898.
 11. A. Concustell, Á. Révész, S. Suriñach, L.K. Varga, G. Heunen, and M.D. Baró, Microstructural Evolution During Decomposition and Crystallization of the Cu₆₀Zr₂₀Ti₂₀ Amorphous Alloy, *J. Mater. Res.*, 2004, **19**(02), p 505–512.
 12. E.S. Park, H.J. Chang, D.H. Kim, W.T. Kim, Y.C. Kim, N.J. Kim, and Y.W. Kim, Formation of Amorphous Phase in Melt-Spun and Injection-Cast Cu₆₀Zr₃₀Ti₁₀ Alloys, *Scr. Mater.*, 2004, **51**(3), p 221–224.
 13. X.F. Pan, H. Zhang, Z.F. Zhang, M. Stoica, G. He, and J. Eckert, Vickers Hardness and Compressive Properties of Bulk Metallic Glasses and Nanostructure-Dendrite Composites, *J. Mater. Res.*, 2005, **20**(10), p 2632–2638.
 14. Q.S. Zhang, W. Zhang, G.Q. Xie, K.S. Nakayama, H. Kimura, and A. Inoue, Formation of Bulk Metallic Glass in situ Composites in Cu₅₀Zr₄₅Ti₅ Alloy, *J. Alloys Compd.*, 2007, **431**(1–2), p 236–240.
 15. E. Ence and H. Margolin, A Study of the Ti-Cu-Zr System and the Structure of Ti₂Cu, *Trans. Metal. Soc. AIME*, 1961, **221**, p 320–322.
 16. A. Raman and K. Schubert, Über die Verbreitung des Zr₂Cu-Typs und Cr₂Al-Typs, *Z. Metallkde*, 1964, **55**(12), p 798–804.
 17. W.R. Chiang, KCh. Hsieh, Y.A. Chang, G. Fan, D. Qiao, D. Qiao, F. Jiang, and P.K. Liaw, Phase Equilibrium in the Cu-Ti-Zr System at 800 °C, *Mater. Trans.*, 2007, **48**(7), p 1631–1634.
 18. U.E. Klotz, Ch. Liu, P.J. Uggowitzer, and J.F. Löffler, Experimental Investigation of the Cu-Ti-Zr System at 800 °C, *Intermetallics*, 2007, **15**, p 1666–1671.
 19. P.G. Qin, H. Wang, L.G. Zhang, H.S. Liu, and Z.P. Jin, The Isothermal Section of the Cu-Ti-Zr System at 1023 K Measured with Diffusion-Triple Approach, *Mater. Sci. Eng. A*, 2008, **476**, p 83–88.
 20. A.M. Storchak-Fedyuk, L.V. Artyukh, L.A. Duma, P.G. Agraval, M.A. Turchanin, and T.Y. Velikanova, Phase Equilibria in the Cu-Ti-Zr System at 750 °C. I. Isothermal Section at the Copper Content 0 to 50 at.%, *Powder Metall. Met. Ceram.*, 2017, **56**(1–2), p 78–87.
 21. A.M. Storchak-Fedyuk, L.V. Artyukh, A.A. Grytsiv, P.G. Agraval, M.A. Turchanin, and T.Y. Velikanova, Phase Equilibria in the Cu-Ti-Zr System at 750 °C. II. Isothermal Section at the Copper Content 50 to 100 at.%, *Powder Metall. Met. Ceram.*, 2017, **56**(3–4), p 220–230.
 22. G.N. Hermana, H.-M. Hsiao, P.-C. Kuo, P.K. Liaw, Y.-C. Li, S. Iikubo, and Y.-W. Yen, Phase Equilibria of the Cu-Zr-Ti Ternary System at 703 °C and the Thermodynamic Assessment and Metallic Glass Region Prediction of the Cu-Zr-Ti Ternary System, *J. Non-Crystal. Solids*, 2021, **551**, p 120387.
 23. R. Arroyave, T.W. Eagar, and L. Kaufman, Thermodynamic Assessment of the Cu-Ti-Zr System, *J. Alloys Compd.*, 2003, **351**(1–2), p 158–170.
 24. M.A. Turchanin, T.Y. Velikanova, P.G. Agraval, A.R. Abdulov, and L.A. Dreval, Thermodynamic Assessment of the Cu-Ti-Zr System III Cu-Ti-Zr System, *Powder Metall. Met. Ceram.*, 2008, **47**(9–10), p 586–606.
 25. M. Yu, *Teslyuk Ternary Intermetallic Compounds with Structure of Laves Phases* L'viv University, L'viv, 1965, p1–16
 26. M.Y. Teslyuk, *Metallic Compounds with Structure of Laves Phases* Nauka, Moscow, 1969, p80
 27. X. Yan, X.-Q. Chen, A. Grytsiv, P. Rogl, R. Podloucky, V. Pomjakushin, H. Schmidt, and G. Giester, Crystal structure, Phase Stability and Elastic Properties of the Laves Phase ZrTiCu₂, *Intermetallics*, 2008, **16**, p 651–657.
 28. A.M. Storchak-Fedyuk, V.M. Petyukh, and L.V. Artyukh, Research of As-Cast Alloys of the Cu-Ti-Zr System, *Curr. Probl. Mater. Sci. Ser. Physicochem. Fundam. Powder Mater. Technol. Kyiv*, 2007, **2007**, p 22–26.
 29. A. Storchak, T. Velikanova, V. Petyukh, A. Samelyuk, V. Sobolev, and M. Bulanova, Phase Equilibria in the Ti-CuTi₂-CuZr₂-Zr region of the ternary Cu-Ti-Zr System, *Powder Metall. Met. Ceram.*, 2022, **61**(5–6), p 337–349.
 30. T. Velikanova and M. Turchanin, Copper-Titanium-Zirconium, Landolt-Börnstein, Numerical Data and Functional Relationships in Science and Technology (New Series), Group IV: Physical Chemistry, in *Ternary Alloy Systems Phase Diagrams Crystallographic and Thermodynamic Data*, Vol. 11C3. W. Martienssen, Ed., Springer, Berlin Heidelberg, 2006, p436–464
 31. I. Ansara and V. Ivanchenko, Cu-Ti (Copper-Titanium), MSIT Binary Evaluation Program, in *MSIT Workplace*. G. Effenberg, Ed., MSI Materials, Hollister CA, 2002
 32. M.A. Turchanin, P.G. Agraval, and A.R. Abdulov, Thermodynamic Assessment of the Cu-Ti-Zr System: II Cu-Zr and Ti-Zr Systems), *Powder Metall. Met. Ceram.*, 2008, **47**(7–8), p 428–446.
 33. V.N. Chebotnikov and V.V. Molokanov, Structures and Properties of Alloys in the Ti₂Cu-Zr₂Cu Section of the Ti-Zr-Cu System in Amorphous and Crystalline States, *Inorg. Mater.*, 1990, **26**(5), p 960–964.
 34. Y.A. Kocherzhinskiy, E.A. Shishkin, and V.I. Vasilenko, The Apparatus for Differential Thermal Analysis with a Thermocouple Sensor up to 2200 °C, in *Diagramy Sostoyaniya Metalicheskikh System*. Nauka, Moscow, 1971, p245–249
 35. V. Massalski, P.R. Subramanian, H. Okamoto, L. Kasprzak, Eds., *Binary Alloy Phase Diagrams: Handbook* 2nd edn. ASM International, Materials Park, OH, 1990, p3589
 36. K.J. Zeng, M. Haemaelaenen, and H.L. Lukas, A New Thermodynamic Description of the Cu-Zr System, *J. Phase Equilib.*, 1994, **15**(6), p 577–586.
 37. P. Villars and L.D. Calvert, *Pearson's Handbook of Crystallographic Data for Intermetallic Phases*, 2nd edn. ASM International, Materials Park, OH, 1991, p3750
 38. J.Z. Jiang, H. Kato, T. Ohsuna, J. Saida, A. Inoue, K. Saksl, H. Franz, and K. Ståhl, Origin of Nondetectable x-ray Diffraction Peaks in Nanocomposite CuTiZr Alloys, *Appl. Phys. Lett.*, 2003, **83**(16), p 3299–3301.

Publisher's Note Springer Nature remains neutral with regard to jurisdictional claims in published maps and institutional affiliations.

Springer Nature or its licensor (e.g. a society or other partner) holds exclusive rights to this article under a publishing agreement with the author(s) or other rightsholder(s); author self-archiving of the accepted manuscript version of this article is solely governed by the terms of such publishing agreement and applicable law.